FRICTION STIR PROCESSING OF $Al_{0.3}CoCrFeNi$ HIGH ENTROPY ALLOY

A THESIS

Submitted in partial fulfillment of the requirements for the award of the degree

of

Master of Technology

by

C. RAMCHANDRA REDDY

DEPARTMENT OF MECHANICAL ENGINEERING

INDIAN INSTITUTE OF TECHNOLOGY INDORE

MAY, 2022

INDIAN INSTITUTE OF TECHNOLOGY INDORE

CANDIDATE'S DECLARATION

I hereby certify that the work which is being presented in the thesis entitled **" Friction Stir Processing of $Al_{0.3}$CoCrFeNi High Entropy Alloy "** in the partial fulfillment of the requirements for the award of the degree of **MASTER OF TECHNOLOGY** and submitted in the **DEPARTMENT OF MECHANICAL ENGINEERING, Indian Institute of Technology Indore**, is an authentic record of my own work carried out during the time period from August 2020 to May 2022 under the supervision of **Dr. Dan Sathiaraj**, Assistant Professor, Department of Mechanical Engineering, Indian Institute of Technology, Indore.

The matter presented in this thesis has not been submitted by me for the award of any other degree of this or any other institute.

R. C. Reddy
01/06/2022

Signature of the student with date
RAMCHANDRA REDDY

This is to certify that the above statement made by the candidate is correct to the best of my/our knowledge.

31/05/22

Signature of the Supervisor

Dr. Dan Sathiaraj

Ramchandra Reddy has successfully given his M.Tech. Oral Examination held on **23rd May 2022.**

31/05/22

Signature of Supervisor of M.Tech. thesis
Date:

Girish

Convener, DPGC
Date: 01.06.2022

Abhijit Ghosh

Signature of PSPC Member
Dr. Abhijit Ghosh
Date: 01.06.2022

01-06-2022

Signature of PSPC Member
Dr. Indrasen Singh
Date:

ACKNOWLEDGEMENTS

I take this opportunity to express my deep sense of respect and gratitude for **Dr. Dan Sathiaraj** for believing in me and providing this golden opportunity and continued support to work under his supervision. His constant encouragement, friendly interactions, and constructive support have enabled this work to achieve its present form. His innovative perspective toward things and his continuous pursuit of perfection have profoundly affected me and transformed me significantly. I would like to thank my PSPC members, **Dr. Abhijit Ghosh** and **Dr. Indrasen Singh**, for their precious guidance and support from the bottom of my heart. Their active interest in my research and insightful discussions have encouraged me to explore deeper and deeper into my research and have greatly aided me in bringing this research to its current state.

I am thankful to IIT Indore for allowing me to carry out the research work and providing all the facilities. I am grateful to the Head of the Department of Mechanical Engineering and the DPGC convener for their assistance and facilities, moral support, and kindheartedness throughout my M.Tech program. It is a great pleasure to acknowledge the support and help extended by **Mr. Pradyumn Kumar Arya**, **Miss. Poonam Deshmukh Suresh**, **Mr. Pankaj Kumar**, and **Mr. Mahesh G Patel** for their assistance and guidance. I want to express gratitude to other members of the Advanced forming research group for their moral support and the friendly nature we have created in our lab.

I can't end these prefatory remarks without expressing my heartfelt thanks and reverence for my lovely parents and their blessings and efforts to keep my morale high throughout my work. Your unmatched support made this work possible.

With regards,

Ramchandra Reddy

DEDICATION

This thesis is dedicated to my parents, who have always encouraged me to pursue my dreams and instilled in me the value of knowledge and perseverance throughout my life.

Abstract

The alloying principle has been developed to obtain the desired properties of materials, which typically involves adding secondary or foreign elements of minor quantities to a primary component. Thus alloys are named after the major component of the alloy, for example, Fe-base, Al-base, and Ni-base alloys. However, in the past two decades, a new alloying strategy that consists of the combination of multiple primary elements in large concentrations led to the development of a new class of metallic materials called High Entropy Alloys (HEAs). Due to this distinct alloying concept, HEAs often exhibit unusual properties compared to conventional alloys. Very few investigations were carried out on multi-dimensional alloys and are primarily focused on experimental analysis. The literature shows that a few high-entropy alloys possess exceptional properties exceeding those of conventional alloys. But enhancing its material properties for engineering applications is a challenge.

One of the primary and effective methods to enhance the material properties of high entropy alloys is through surface modification. The Friction stir process (FSP) is one of the effective processes for improving material properties by microstructural modification. The mechanical and microstructural properties are controlled by processing parameters like rotational and translational speeds. In the present study, FSP is carried out on $Al_{0.3}CoCrFeNi$ High entropy alloy, using two different tool geometries (i.e., cylindrical and square-shaped) by varying the process parameters, mainly tool rotational speed and traverse speed. A numerical study was performed using ABAQUS CAE finite element software to understand the complex thermo-mechanical process involved with friction stir processing. The simulation primarily aims to study the effect of process parameters and tool geometry on the HEA workpiece.

The Johnson-Cook material model is utilized to obtain the stress and strain distribution on the workpiece. The temperature distribution over the plate was obtained by penalty-based frictional contact between the tool and the plate. The model also observed a change in material flow behavior as shoulder geometry changed. An experimental study on the above model was also conducted to understand the computational model's potential deviations compared to the real-time experiments. The experimental setup acted as a measure to validate selected model results to understand its ability to replicate the actual phenomenon.

Keywords: Friction stir Processing, High Entropy Alloys, Temperature distribution, Flow Stress, ABAQUS/CAE.

LIST OF PUBLICATIONS

1. **Ramchandra Reddy**, Pradyumn Arya, Pankaj Kumar, Dan Sathiaraj, N.K. Jain; Friction Stir Welding of Lightweight Dissimilar Materials and Alloys (2022)- *Laser Applications in Manufacturing: CRC Press, a Taylor and Francis Group (Apple Academic Press)*. (Accepted).

2. **Ramchandra Reddy**, Dan Sathiaraj; Friction Stir Processing of $Al_{0.3}CoCrFeNi$ High Entropy Alloy (2022)- *2^{nd} International Conference on Advance in Materials and Manufacturing Technology: NIT Bhopal* (Abstract Submitted).

TABLE OF CONTENTS

LIST OF FIGURES

LIST OF TABLES

NOMENCLATURE

- FSP – Friction Stir Processing
- HEA – High Entropy AlloyIn-wheel motor electric vehicles
- SPD – Severe Plastic Deformation
- TMAZ – Thermo-mechanically affected zone
- HAZ – Heat affected zone
- SZ – Stir/Stirring zone
- BM – Base Metal
- C-800 – Cylindrical pin profile at 800 rpm
- C-1000 – Cylindrical pin profile at 1000 rpm
- S-800 – Square pin profile at 800 rpm
- S-1000 – Square pin profile at 1000 rpm

Chapter 1

Introduction

1.1History and Background

Over thousands of years, humankind has strived to produce numerous modern materials [1], exploring contemporary metals and making new alloys which have played a crucial part in many developments. From the time of the Bronze Age, alloying principles were created. Many conventional alloys have been developed as a result of the alloying principle, which is mainly dependent on principle elements. About 30+ practical conventional alloys have been developed, for example, steels (Fe-based), Al, Cu, Ti, Mg, Ni alloys, and so on. [2]. These alloys are developed based on the principle base-element paradigm, i.e., the alloys include one or rarely two principle base elements, and tiny amounts of foreign elements are added to enhance or modify material properties. Thus, the principle base-element paradigm restricts their Composition and the evolution of novel properties. Currently used, most of the high-performance alloys were being developed in the 1960s. Since then, numerous approaches have been carried out to address the ongoing need for advanced applications with improved material properties[3].

One such approach to boost the material properties of conventional alloys is novel processing techniques like thermo-mechanical treatments, high strain rate forming, equal-channel angular processing, friction stir processing, rapid solidification, and surface treatments. Another approach developed by Yeh et al. is to vary the composition of the alloys, which led to the development of new intermetallic compounds and their alloys.

Many kinds of research are being carried out on combining both processing and compositional techniques to satisfy the current need to develop materials with superior properties. The key objectives in alloy research are to obtain materials with High strength, toughness, hardness, stiffness, wear resistance, oxidation resistance, elevated temperature strength, corrosion resistance, formability, lightweight, good magnetic properties, and environment friendly. The conventional alloys met the requirements mentioned above. However, there is still a massive demand for material improvements in various applications, such as Aerospace & automotive engines, nuclear & tool materials, light materials with superior properties, functional coatings, superconductors, and high-temperature refractory materials [4-8]. To overcome the marginal returns from conventional alloys in meeting the above requirements, about one and a half decades ago, Yeh et al. and Cantor et al. caught researchers' attention based on the concept of multiple principle elements design [9].

In contrast to the principle base-element paradigm, a new alloying strategy was developed, which involves combining multiple primary elements in an equimolar or relatively close proportion to form a unique family of metal alloys called High Entropy alloys (HEAs). Due to this distinct alloying concept, HEAs often exhibit unique properties compared to conventional alloys. HEAs are increasingly studied because of their novel properties [2,4–8]. HEAs possess excellent mechanical properties than traditional alloys in terms of hardness, strength, wear, and oxidation resistance, which are appealable in various fields like automotive, industrial applications, aerospace industry, etc. Furthermore, high entropy alloys do not require any particular equipment for fabrication, indicating the enormous potential for large-scale production and vast applications

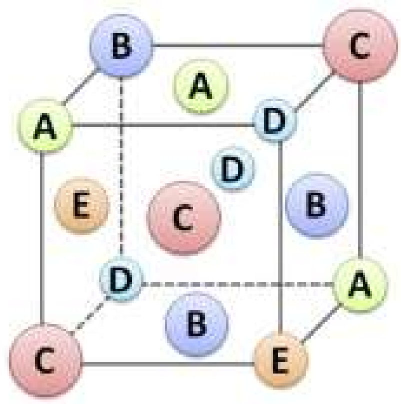

Fig. 1.1: FCC: Schematic representation of High entropy alloys
(5 principle elements)

1.2 Definition of HEAs

1.2.1 Definition based on Composition:

There is no well-defined definition for "multicomponent alloys", whereas several explanations exist for High entropy alloys. From the literature, High entropy alloys are referred to as novel materials consisting of equimolar or nearly-equimolar compositions of at least five major alloying elements. The above definition merely specifies elemental concentrations and sets no limits on entropy magnitude [10].

1.2.2 Definition based on Entropy:

Boltzmann's equation from thermodynamics relates the configurational entropy & the system's complexity. The configurational entropy that for each mole of a solution consisting of n components, each with molar fractions of X_j can be expressed as [9,12]:

$$\Delta S_{\mathrm{conf}} = -\,R \sum_{j=1}^{n} \left(X_j \ln X_j \right) \tag{1}$$

Where,

R = Molar gas constant

X_j = mole fraction = $\dfrac{\text{Amount of a particular element in a solution (in moles)}}{\text{The total amount of all elements in a solution (in moles)}}$

Therefore [13],

$$\Delta S_{conf} = - R \left(\frac{1}{n}\ln\frac{1}{n} + \frac{1}{n}\ln\frac{1}{n} + \frac{1}{n}\ln\frac{1}{n} + ... + \frac{1}{n}\ln\frac{1}{n}\right)$$

$$\Delta S_{conf} = - R \left(\ln\frac{1}{n}\right) = R \ (\ln n) \tag{2}$$

From the above equation, it is clear that as the number of elements in the solution increases, ΔS_{conf} increases.

For n = 4 , ΔS_{conf} = R (ln 4) = 1.39R

n = 5 , ΔS_{conf} = R (ln 5) = 1.61R

n = 6 , ΔS_{conf} = R (ln 6) = 1.79R

n	1	2	3	4	5	6	7	8	9	10	11	12
ΔS_{conf}	0	0.69R	1.1R	1.39R	1.61R	1.79R	1.95R	2.08R	2.2R	2.3R	2.4R	2.49R

Table 1.1: ΔS_{conf} for different number of elements in a system [3]

Based on the number of elements in the system & ΔS_{conf} , the multicomponent alloys are classified as Low, medium, and high entropy alloys.

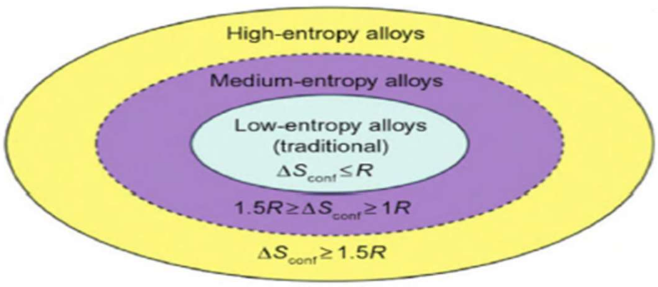

Fig. 1.2: Classification of Multi-component alloys based on ΔS_{conf} [3]

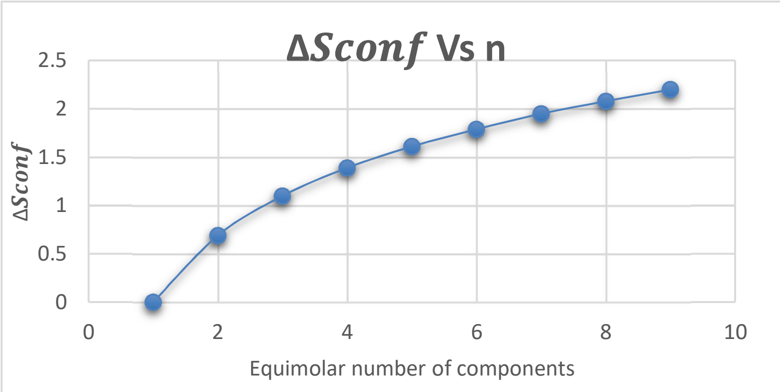

Fig. 1.3: Change in ΔS_{conf} as a function of n [4]

1.3 Severe Plastic Deformation

Since ancient times, improving the material properties has been a primary focus of the research community for advanced applications. The mechanical characteristics of materials depend on their microstructure. The Hall-Petch equation shows that a material's strength is proportional to its grain size [14].

$$\sigma_y = \sigma_o + kd^{\frac{-1}{2}}$$

Where d = grain size , k = constant and σ_o = friction stress

Thus to achieve the high strength of an alloy, refine (reduce) the grain size. Since then, attempts have been made to improve the material characteristics by inducing deformation, and many processing techniques like rolling, forging, extrusion, etc., are being developed.

The process of inducing deformation is referred to as "Metal forming." The von Mises plastic strain imposed in traditional metal forming techniques, including rolling, forging, and extrusion, is typically less than 2.0. Thus induced deformation refines the microstructure from coarse to ultra-fine (sub-microns) size grains. Nonetheless, the grain size obtained by this method is generally in the range of 1 – 10 µm, which is significantly insufficient to boost the strength. Therefore, multiple passes of rolling, drawing, and extrusion are carried out for further refinement of grains up to a nano-level by applying the Von-Mises plastic strain of > 2 [15]. But by undergoing multiple passes, the dimensions could be altered, i.e., thickness and diameter become very small. The Severe Plastic Deformation (SPD) approach is employed to overcome the above concern.

The metal processing techniques that enable the refinement of microstructure under plastic deformation to extreme strains that are difficult to achieve with conventional metal forming processes are known as Severe plastic deformation techniques [16]. Severe plastic deformation has drawn researchers' interest over the last two decades owing to its ability to achieve bulk nano or ultrafine-grained microstructure. In the newly developed technique, the material is subjected to severe plastic deformation (Von-Mises plastic strain >2), which refines the grains to sub-micron levels [17]. This is the leading technique that produces ultrafine-grained materials from coarse-grained (>100 μm) through multiple passes of plastic deformation.

SPD is accomplished when the material is plastically deformed repeatedly without changing the original shape and dimensions, which means the effective plastic strain in each step gets added to the next step, thus resulting in significant plastic strain [18]. The materials subjected to SPD exhibit exciting and distinct properties that are not observed in typical coarse-grained materials. Several processing techniques that have been developed for achieving SPD are:

- ✓ Equi-channel angular pressing (ECAP).
- ✓ Torsion or shear under high pressure.

  Examples: High-Pressure Torsion, High-Pressure Sliding,
  Friction Stir Processing
- ✓ Direct/indirect extrusion

  Examples: Simple Shear Extrusion, Twist Extrusion, etc.,

- ✓ Pressing/Forging

  Examples: Constraint Groove Pressing, Repetitive forging (RF)
- ✓ Based on rolling
- ✓ Combined SPD techniques

1.3.1 Severe Plastic Deformation of High entropy alloys

As discussed in earlier sections, HEAs exhibit unique properties compared to conventional alloys. HEAs possess superior mechanical properties like strength, hardness, wear, and oxidation resistance than traditional alloys, which are attractive in many fields. The mechanical behavior of materials can be further enhanced by thermomechanical treatment. Nano-level grains can be achieved in HEAs alloys using the Severe plastic deformation technique, and, in particular, Frictions stir processing has been used.

1.4 Friction Stir Processing

One cannot find all the required properties in one material. In many applications like the aerospace industry, automotive industry, structural construction, etc., the selection of materials with specific properties plays a significant role. Thus alloying principle has been developed to meet some requirements. However, processing those alloys with particular properties like high strength and hardness has constraints on production cost and time. The materials with fine and homogeneous grain sizes and structures possess high strength and ductility. Hence, developing a technique that produces a material with the requirements mentioned above at low production cost and time is necessary. Thus new techniques like Equi-channel angular pressing, Friction stir processing, High-pressure Torsion, Simple shear extrusion, Twist Extrusion, and so on were developed. In this research, friction stir processing is employed to refine the grains of a microstructure which, in return, increases the strength and hardness.

1.4.1 Working Principle of Friction Stir Processing

Friction stir processing is a derivative of R.S.Mishra and Co's invention of friction stir welding (FSW) in 1999 [19]. FSP works similarly to FSW, but instead of joining the metals modifies the microstructure. This new process is one of the exciting techniques for enhancing properties and modification of microstructure. The following is the basic working principle of FSP: A non-consumable tool with a pin of small diameter concentric with a larger diameter shoulder rotating at a very high speed is penetrated into the plate (workpiece). The friction between the plate and tool generates significant heat energy. The frictional heat yielded results in softening of a material. When the tool's shoulder touches the plate, the softened material plastically deforms severly and is recrystallized because of the stirring effect of probe. Therefore, a more refined and more homogeneous microstructure could be achieved.

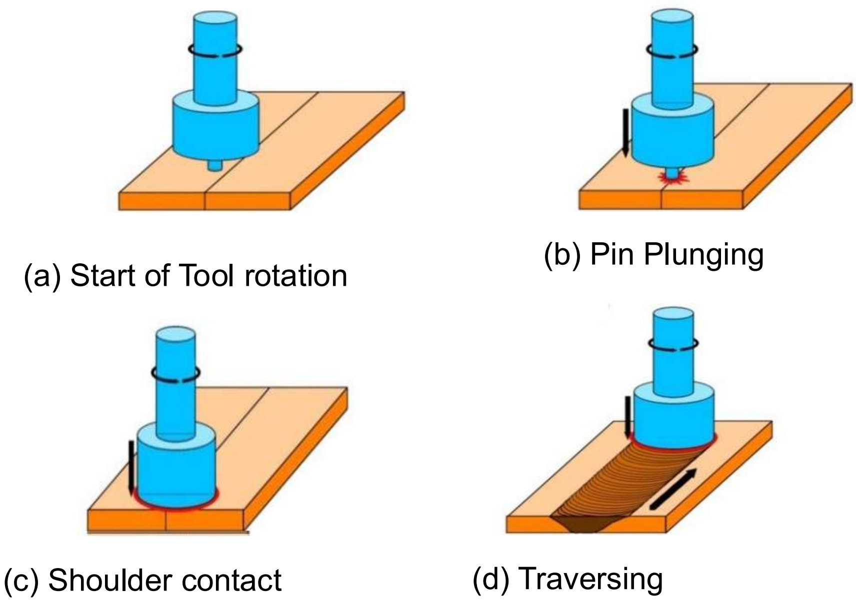

Fig. 1.4: Steps involved in FSP [4]

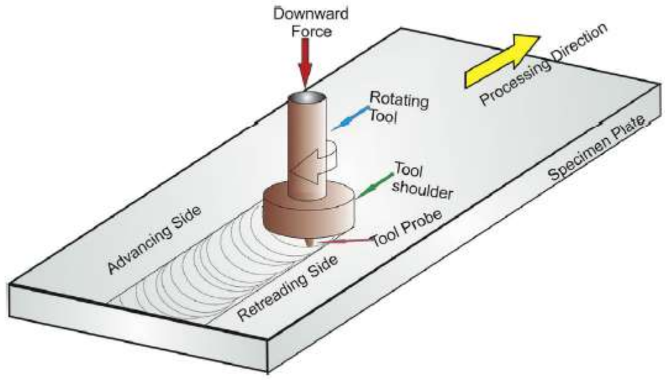

Fig. 1.5: Schematic representation of FSP [5]

The microstructure evolved during FSP is owing to plastic deformation, material flow, & rise in temperature characterized by a stirring region surrounded by a thermo-mechanical affected zone (TMAZ), heat-affected zone (HAZ), and base metal zone [20]. The plastically deformed material transfers from the tool's retreating side (RS) to the advancing side (AS). It is later forged by the tool's shoulder, causing the material to undergo significant state modification. In the FSP process, the processed area and TMAZ are primarily interested areas. This area determines the properties of the processed zone, specifically adhesion.

1.4.2 Process Parameters of FSP

The process parameters have a significant impact on obtaining the desired microstructure in a processed area. The process parameters of FSP should be selected with utmost care to ensure that a sufficient amount of heat is generated and stirring is performed for plastic deformation & recrystallization. The FSP's process parameters are generally classified into three major types: Machine variables, Tool design variables, & Material Properties. The selection of process variables depends on the material properties of the workpiece. High-melting point alloys require more heat input for softening and recrystallization.

Mechanical characteristics like hardness, yield strength, and ductility of the workpiece regulate plastic deformation [21,22]. For higher thermal conductivity alloys, larger heat input is necessary for a defect-free stirring zone [23].

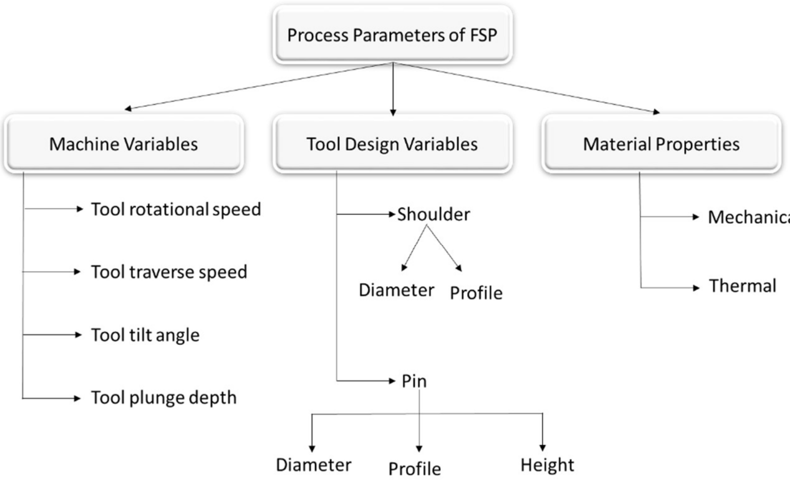

Fig. 1.6: Classification of FSP Process Parameters

1.4.3 Effect of Machine Variables

The rotational and transverse speeds of the tool are primary process parameters of FSP. The slight change in the combination of these process parameters may end in defects in the processing zone. The friction between the plate (workpiece) & the tool generates the heat required for plastic deformation and recrystallization. The mechanical properties directly depend on the evolution of microstructure and plastic deformation, which are affected by the amount of heat generated. The amount of heat generated directly depends on rotational speed and is inversely reliant on transverse movement, affecting resultant properties [24]. As the heat generated is lower, grain refinement will be more and vice-versa, but a sufficient amount of heat must be generated for material softening [25]. The plunge rate and tool tilt angle also affect the stir zone but are assumed constant. Thus optimum parameters are considered for a defect-free processing zone.

The empirical relationship between the rotational speed (ω), transverse speed (v), and maximum temperature (T_{max}) is proposed as [26]:

$$\frac{T_{max}}{T_{MP}} = \mathrm{K}\left(\frac{\omega^2}{v * 10^4}\right)^{\alpha} \tag{3}$$

Where,

K = 0.64 and 0.76, α = 0.039 to 0.062 and T_m (◦ C) = Alloy melting point.

1.4.4 Effect of Tool Design Variables

The shoulder & pin are the primary tool design variables. The tool's geometry influences material softening, heat generation, and the resulting microstructure [27]. The tool's geometry mainly includes the profile and diameter of both shoulder and pin. The pin's length depends on the thickness of the workpiece, and it should be less than the workpiece's thickness. Machine (ω *and* v) and tool design variables affect the material flow behavior in the processing zone [28]. The following figure illustrates the best tool design for obtaining a good processing zone from the literature.

Generally, the concave-shaped bottom surface of the tool shoulder is utilised as it prevents the escape of the volume of softened material from the pin in the processed zone. It is necessary to provide the tilt angle to keep the softened material under the shoulder surface. Usually, a tilt angle ranging from 1-3^{o} is supplied to the tool. The geometry of the shoulder determines the amount of heat produced. As the shoulder diameter gets bigger, the processing zone & heat generation grows, further enhancing the material flow behavior. So far, various pin profiles like hexagonal, cylindrical, square, tapered-cylindrical, threaded-cylindrical, triangular, etc., have been utilised. It has been observed that the wear rate of a square probe is greater than that of a cylindrical probe as the sharp corners of the square tool are rapidly deteriorated. In the current study, square and cylindrical pin profiled tools are adopted for FSP.

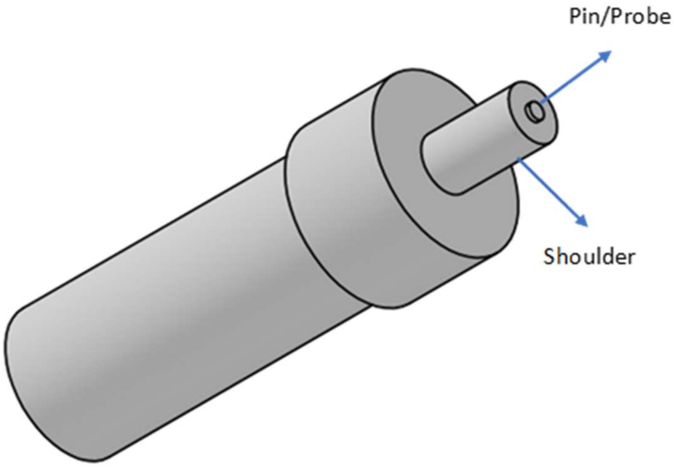

Fig. 1.7: FSP Tool Geometry

1.4.5 Advantages of FSP

In comparison to other metal processing methods, FSP possesses numerous and distinct advantages. They are:

- FSP does not modify the dimensions and shape of the processing components.
- FSP is a versatile technique that may be used to manufacture, process, and synthesise materials with a wide range of applications.
- FSP is a solid-state processing approach that accomplishes grain refinement of microstructure, uniformity, and densification in single-step processing.
- The processing zone's mechanical behavior and grain refinement are precisely controlled by process parameters of FSP like the tool's rotating and traversal speeds, optimum tool design, & active cooling.

- The depth and area of the FSPed area can be altered by adjusting the tool's pin length and shoulder diameter, which is difficult in other metalworking techniques.
- In FSP, the heat required for processing comes from friction and plastic deformation. Thus making it a green and energy-efficient approach without emission of noise, toxic gases, and eradiation.

1.4.6 Applications of FSP

- FSP can be used to eliminate many of the flaws in the casting process, such as porosity & microstructural defects.
- The microstructural characteristics of powder metal objects can also be improved by friction stir processing.
- FSP can also make metal matrix composites.
- FSP could be utilised to modify the microstructure and boost the mechanical characteristics of metallic materials.

1.5 Organization of the Thesis

The following chapters make up this thesis:

Chapter 1: Brief history and background of High entropy alloys, Working principle of FSP, the effect of process parameters, applications, and advantages of FSP.

Chapter 2: The literature review of the past work, identified research gap, and research statement formulation.

Chapter 3: Experimental procedure, the plate material section, tool material selection, and design.

Chapter 4: Overview of numerical methods, the step-by-step procedure followed in the modeling, and solver types.

Chapter 5: Results and discussions of the numerical model and experimental analysis and validation of results**.**

Chapter 6: Conclusions and Future Scope of the research

Chapter 2

Literature Review and Research Statement

In the field of welding, the friction stir technique is a real game-changer. In the weld zones, this novel process generates very tiny grains. If this can be employed as a processing technique, it will likely substitute the current conventional, sophisticated, and costly methods. The property of the friction stir region led to the creation of FSP, a revolutionary thermos-mechanical material processing method that is both inexpensive and energy-efficient. FSP is a relatively new approach, so minor literature is available than FSW. This chapter presents an overview of the research carried out to date in the area of Friction stir technology. Initially, FSP was carried on Al and Mg-based alloys. After the development of HEAs, FSP has been extended to them. Various experimental and numerically modeled methods of FSP are discussed.

2.1 Past work on the Mechanical properties and Process parameters

[Pathak et al. 29] explored the FSW of aluminium-5754 sheets. The main objective was to analyse the impact of process parameters like rotating speed, pin profile, plunge rate, and an idle period on temperature distribution, microstructure, and weld strength. The results reveal that the peak temperature rises with the tool's rotational speeds for both cylindrical and tapered pin profiles. The friction heat generated using a cylindrical pin was more significant during FSW than the tapered pin profile. It was observed that shear loads rose as plunge depth, rotating speed, and dwell duration increased.

[Yutaka S. Sato et al. 30] explored the FSW of Aluminium 6063-T5 alloy. The main objective is to examine the impact of tool's rotational speed on the microstructural evolution and hardness. It was noticed that as the rotating rate increased, the peak temperature during FSW rose. As the peak temperature increases, the grain refinement will be more, i.e., grain size increases. Therefore, the rotational speed directly influences the increase in grain size.

[Devinder Yadav et al. 31] explored the FSP of pure Aluminium. The main objective is grain refinement & understanding of the microstructure's evolution and its influence on the material properties. The results reveal that substantial grain refinement and equiaxed, refined grains are observed in a single pass. The strength and hardness of the alloy are increased massively without a change in ductility.

[B.M. Darras et al. 32] examined the FSP of commercial AZ31-magnesium alloy. The main objective was to understand the alloy's microstructural behavior, temperature distribution, and hardness after FSP. The results suggest that very fine grain sizes and microstructure homogeneity were obtained in a single pass.

[Xiuli Feng et al. 33] studied the FSP of aluminum 2219-T6 alloy by utilizing a unique submerged processing approach to enhance cooling. The main aim was to investigate the microstructural characteristics and micro-hardness in the FSPed zone with respect to changes in rotational speeds and at constant traverse speed. The grain size of the FSPed area was significantly lower than the base metal. The micro-hardness of the stirring zone was observed to diminish as the rotating speed increased.

[Xiaomeng Qin et al. 34] studied the FSW of CoCrFeNi plates under various normal forces and rotational speeds. The main focus was to understand the impact of process parameters on grain refinement, mechanical characteristics, and microstructure evolution. The stir zone possesses uniform recrystallized grains, and the thermomechanically affected area possesses partially recrystallized grains. The grain size in the processed area increases with the rotating speed of the tool. Differences in grain size and composition are observed in SZ as onion-ring or fish-bone shapes with varying rotating speeds. The grain refinement in the stirring zone improved the mechanical characteristics of the welded plates, like the tensile strength & hardness.

[Sam Yaw Anaman et al. 35] investigated the impacts of FSP on CoCrFeNiMn HEA & associated electrochemical behavior by examining the microstructures at multiple locations across the processed zone in Na_2SO_4 electrolyte solution using potentiodynamic polarisation. Also, the pitting corrosion phenomenon of the processed area was evaluated by both finite element (COMSOL Multiphysics) and experimental approaches. The analysis reveals that very fine grain size is inspected in the microstructural examination, and the stir zone with refined grains decreases from top to bottom. Excellent corrosion characteristics are observed due to the creation of Cr_2O_3 passive layer.

[Ning Li et al. 36] studied the FSP of CuCoCrFeNi HEA alloy. The main intention was to know the viability of FSP on HEAs, enhance mechanical properties, and understand the relationship between microstructure and mechanical characteristics in the FSPed area. FSP enhanced the material's hardness and yield strength by over 1.5 times over the base material.

[Feng Xiong et al. 37] worked on the FSP of CoCrFeMnNi HEA with and without nitrogen addition. The research objective was to examine the impacts of FSP and nitrogen addition on the mechanical behavior and microstructural evolution of HEA. The addition of nitrogen efficiently boosts the ultimate tensile and yield strengths of the HEA. After FSP, the grain sizes of the HEA with and without the addition of nitrogen were 7.6 and 2.5 μm, respectively. The mechanical properties like yield strength

(493 MPa), UTS(832 MPa), and uniform elongation(32.6%) of nitrogen added CoCrFeMnNi HEA and FSP possess superior properties to the FSP of CoCrFeMnNi HEA. Solid solution strengthening via adding nitrogen & grain- boundary strengthening via FSP could explain these gains.

[Komarasamya et al. 38] studied the FSP of $Al_{0.1}CoCrFeNi$ HEA. The main objective was to understand the microstructure evolution and grain refinement in the FSPed area at multiple locations using Scanning electron Microscopy(SEM) and their impact on the mechanical behaviour. The grain refinement from millimeters to 0.35-0.15 μm was accomplished using FSP. After the grain refinement, yield strength improved by a factor of 4 while sustaining a significant homogeneous % of elongation, according to the Hall-Petch relationship.

2.2 Past work on the Finite Element Model / Simulations

[S. Z. Aljoaba et al. 39] studied the numerical model using STAR CCM+CFD commercial software of FSP. The main objective of the 3D CFD model is to predict the temperature profiles, strain rate values, grain size, material flow behavior, and dynamic viscosity values. The temperature significantly impacts grain size, which is influenced by process parameters like the rotational and traverse speeds. The rotational speed significantly impacts strain rate values; as it rises, so does the strain rate. The maximum values were found towards the tool's shoulder's an outside edge, where the temperature and material speed values were maximum.

[M Iordache et al.40] studied the finite element model of FSW in ABAQUS/Explicit. In FEM analysis of the processes which involve excessive deformation, Lagrangian elements distort, and solutions may not be accurate. To mitigate severe mesh deformation, many modeling approaches are commonly used. One such method used is Coupled

Eulerian-Lagrangian technique which allows excess deformations. The CEL modeled FE results are validated with experimental results.

[Arindam Baruah et al.41] simulated the plunge stage of the FSW in ABAQUS to understand the complex behavior involved in it. The plunging stage is recognized as the vital step in the FSW because it comprises transient & dynamic material-flow behavior. The excessive deformation error is eliminated using a multiple sections mesh partition & the Adaptive re-meshing(ALE) technique. The results suggest that the amount of frictional heat generated increases till the end of the plunging step and subsequently drops in the dwelling step. The Von-mises stress was observed to rise at the start of tool penetration and fell in the subsequent step times, confirming the phenomena of material softening at higher temperatures.

[Z. Zhang et al. 42] developed the finite element model of FSW using ABAQUS/Explicit commercial software. The goal is to model the temperature profile and material flow behaviour and the impact of process parameters. To solve the problem of excessive deformation Arbitrary Lagrangian-Eulerian (ALE) technique is adopted. The results obtained are: As the tool's rotating speed is increased, the peak temperature rises. Increasing the rotation speed and lowering the welding speed simultaneously can boost the stirring effect in the nugget zone, enhancing the quality of the weld. The rotational speed must be raised synchronously with the welding speed to eliminate the probability of welding defects. If both welding and rotational speeds are increased simultaneously, that can increase residual stress.

[Emad Eldin M. KISHTA et al. 43] developed the finite element model of FSW in ABAQUS/Explicit to predict the influence of process parameters like rotating and traversal speeds on the temperature profile over the workpiece. Initially, all the three parts (plate, backing plate, and tool) were developed by the Lagrangian approach. A very fine mesh is required to avoid distortion for the processes which involve excess deformation. This increased the computational cost drastically. To solve the challenges above, Coupled Eulerian-Lagrangian approach was adopted to model FSW. The results reveal that the maximum temperature increased on both the advancing & retreating sides as the rotating speed increased.

2.3 Identified research gaps

High entropy alloys are novel materials with mechanical properties like superior strength, hardness, wear, and oxidation resistance compared to conventional alloys, which are attractive in many fields. HEAs can replace many existing conventional materials in various industrial applications owing to their unique characteristics. However, very few researchers attempted to obtain ultrafine or nanoscale crystal structures of HEAs. The literature shows that FSP is one of the practical processes for microstructural modification; FSP can achieve an equiaxed uniform grain structure. In order to achieve the necessary grain refinement, it is critical to specify the tool geometry and process parameters like rotational and translational speeds in FSP.

So far, very few have attempted to improve the HEA's mechanical properties and microstructural behaviour. Many researchers have emphasized on FSP-based experimental investigation of HEAs. There is very little work in the literature on the finite element modeling of FSP on High Entropy Alloys(HEA). The process parameters play a vital part in obtaining defect-less processed area. As a result, optimizing the process parameters is essential. The research on the FSP of HEAs is still not well explored. FSP is a complex thermo-mechanical process. It is crucial to comprehend the dynamic material flow and thermal behaviour during FSP. The finite element model provides the flexibility to understand the process better. The relation between the process parameters like shoulder profile, pin profile, plunge rate, rotating, and traversal speeds on the temperature distribution, stress, and strain fields can be adequately understood. The experimental validation of FE results allows for a better understanding of the numerical model's accuracy. The obtained results are compared to the experimental findings for further correlation with microstructure.

2.4 Objective and Methodology of the present research

The current study focuses on the finite element analysis & experimental study of the FSP of $Al_{0.3}CoCrFeNi$ HEA. The numerical modeling was created using ABAQUS/Explicit commercial software. The main objective is to analyse the impact of the process parameters on the microstructural evolution, temperature profile, mechanical characteristics, and residual stresses of the stir zone. The impact of the pin profile was also studied. The cylindrical and cuboidal pin profiles are utilised to comprehend the material flow characteristics. To determine the accuracy of the numerical model, the resulting FE results are compared to the experimental data.

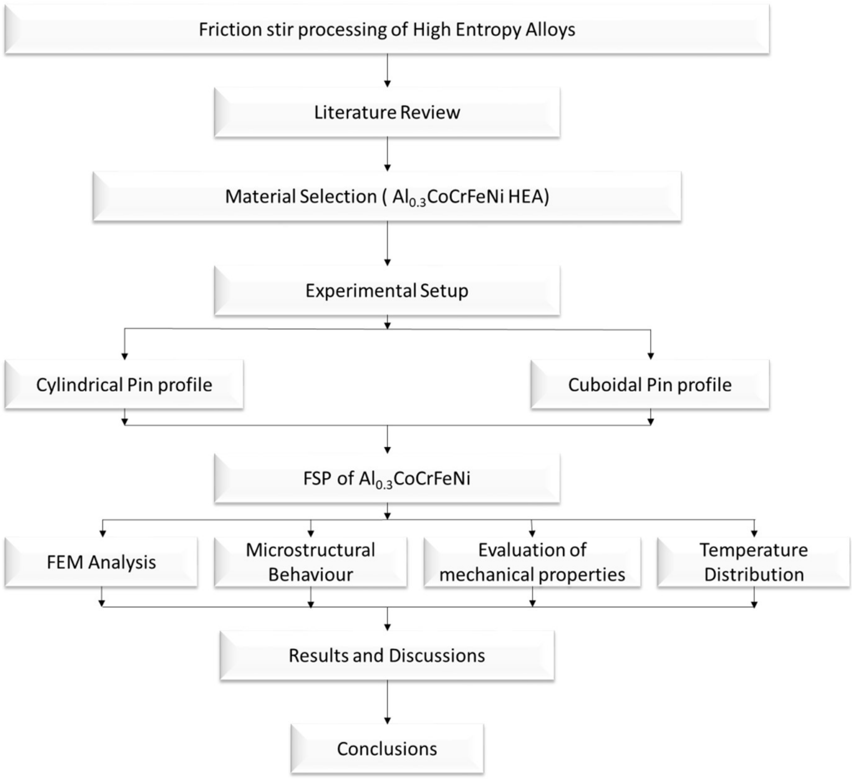

Fig. 2.1: Research Methodology

Chapter 3

Experimental procedure of FSP

This chapter describes the procedure followed for experimentation of FSP, selecting workpiece material (i.e., HEAs), considering their rapid evolution in recent years, tool design, investigation of mechanical behavior like microstructure, tensile strength, hardness of the processed zone, and set up for experimentation. In this research, our focus is to analyze the effects of FSP process parameters and their role in heat generation and microstructure evolution experimentally.

3.1 Experimental setup of FSP

In the current research, a CNC (computer numerical control) milling machine is modified as an FSP machine used to process HEAs. The workbench moves in all three transverse directions (i.e., i, j & k). The tool is mounted in the machine's spindle, which rotates by a motor at a very high speed. During the tool plunge, large forces are exerted on the workpiece as it rotates very fast. So it is essential to clamp the workpiece properly. A specially built fixture with bolts and clamping plates is used to restrain the relative motion of the plate (workpiece) in all directions.

The clamping plates are placed at the bottom and the edges of the workpiece. The process parameters like plunge rate, rotating, and traversal speeds are fed to the machine through the computer. The tool is progressively inserted into the workpiece until its shoulder touches the plate. The dwell time is provided to the tool for the uniform softening of a material. The tool is then moved in the required direction for processing. The temperature distribution over the workpiece is captured using a pyrometer with a sensitivity of 41 $\mu V/^{o}C$. The captured data is examined in the LabVIEW software in the connected computed.

Fig. 3.1: Experimental setup of FSP

Fig. 3.2: Workbench and clamping

3.2 Selection of workpiece material

HEAs are a novel family of metals with many applications in aerospace, automobile, and structural uses owing to their higher elevated temperature strength, oxidation resistance, wear resistance, hardness, etc. HEAs exhibit unique properties compared to conventional alloys by shifting the alloying principle from a single principle element to multicomponent components.

In the current study, FCC-based $Al_{0.3}CoCrFeNi$ high entropy alloy is considered. This HEA displays a wide range of mechanical properties at different temperatures and behaves like a conventional FCC alloy with high flow stress and work hardening in the plastic zone. The percentage of aluminum plays a crucial role in the alloy's microstructure. In the $Al_xCoCrFeNi$ high entropy alloy family, the microstructure of the alloy changes with the ratio of Al.

The microstructure of the $Al_xCoCrFeNi$ HEA is as follows:

For $x < 0.3$ ----- FCC microstructure (Single phase)

$0.3 < x < 0.9$ ----- FCC + BCC microsture (Dual phase)

$X > 0.9$ ----- BCC microstructure (Single phase)

The mechanical properties of $Al_{0.3}CoCrFeNi$ alloy are as follows:

Density	Young's Modulus	Poison's ratio	Specific Heat	Thermal Conductivity	Micro-Hardness
7860 kg/m^3	205 GPa	0.29	460 J/Kg-K	5.989 W/m-K	155 HV

Table 3.1: Mechanical properties of $Al_{0.3}CoCrFeNi$ alloy

Fig. 3.3 Workpiece of $Al_{0.3}CoCrFeNi$ alloy

Al	Co	Cr	Fe	Ni	Total
6.82	24.93	22.57	24.62	21.07	100

Table 3.2: Chemical Composition of $Al_{0.3}CoCrFeNi$ alloy

3.3 Tool material selection and Design

As discussed in the previous sections, the strength and hardness of the tool must be greater than the workpiece to be processed. So tungsten carbide cobalt (WC) tool is used for FSP. The tool is fabricated on the standard CNC lathe machine and diamond grinder. The tool's shoulder's bottom surface is made flat to reduce fabrication complexity. The current study uses the pin of two different geometries for processing, namely circular and square profile pins. The pin's length must be smaller than the workpiece's thickness. The shoulder diameter (D_s) depends on the thickness of the workpiece (t) and can be obtained as $Ds = 6.99 + 2.26\ t$. The literature suggests that the shoulder-to-pin diametrical ratio must be 3 to 3.5.

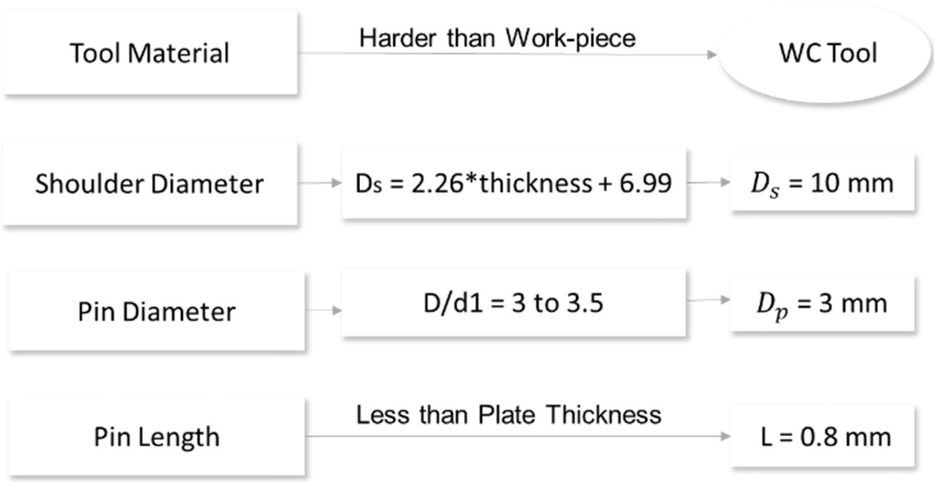

Fig.3.4: FSP Tool Design

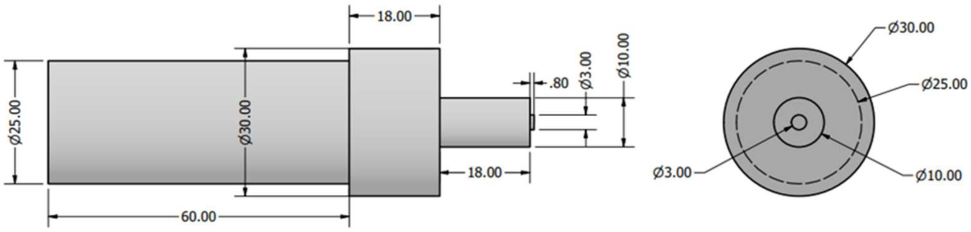

Fig. 3.5: FSP Tool with Circular Cross-Section

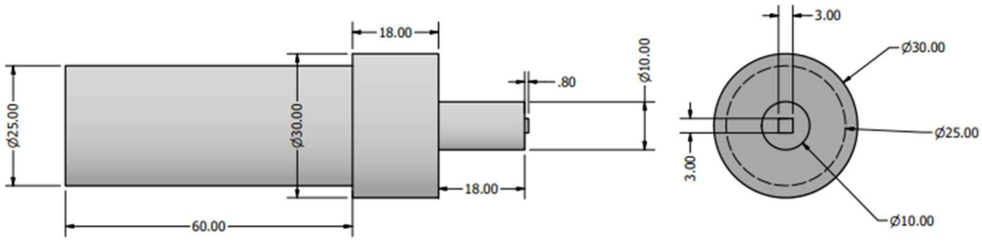

Fig. 3.6: FSP Tool with Square Cross-Section

Fig. 3.7: WC Tools used for FSP

3.4 Selection of Process Parameters

The process parameters have a significant impact on the resulting processed zone. The microstructural characteristics, strength, & hardness are affected by process parameters. An optimum combination of process parameters should be chosen to obtain a defect-less processing zone. The tool's traverse speed and plunge rate are kept constant in the current set of experiments. The rotating speeds of 800 and 1000 rpm are used, and FSP is carried with two different pin geometries at mentioned speeds. To establish the optimal process parameters, several trial tests are conducted. A total of 4 experiments are conducted on the actual workpiece sample by using the air cooling method.

Fixed Process parameters	
Cooling Type	Air Cooling
Tool traverse speed (mm/min)	20
Plunge rate (mm/sec)	0.4
Work piece material	$Al_{0.3}CoCrFeNi$
Tool material	WC
Shoulder dia. (mm)	10
Pin length (mm)	0.8

Variable process parameters	**Values**
Rotational speed (rpm)	800,1000
Pin geometry and dimensions	Cylindrical (3mm dia.) and cuboidal (3 mm side)

Expected results	
Temperature Distribution	: by Pyrometer
Mechanical properties	: Micro hardness , Ultimate tensile strength (UTS)
Metallurgical characteristics	: Microstructure and chemical composition

Table 3.3: Process parameters used for FSP

3.5 Experimental Procedure of FSP

The HEA workpiece is fixed correctly in the fixture using clamping plates, nuts, and bolts such that the relative motion is restrained in all directions during FSP. Generally, FSP involves three major stages: Plunging, dwelling, and processing. In the Plunge stage, the tool is positioned in the required area, and the tool rotating with specified rpm is slowly penetrated into the plate till the shoulder touches the plate. In the dwelling stage, the tool is kept idle for a few seconds such that friction generated between two contact surfaces is converted into heat which is primary in FSP. In the processing stage, the tool is moved at constant speed along the required direction for processing. The material softens and deforms plastically due to frictional heat. The softened material is moved to the tool's backside from the front side.

The process parameters like pin length, profile, and shoulder profile are important process characteristics that affect the material flow & rise in temperature, thus affecting the evolution of microstructure in the processed area. The same procedure is followed by two different tool pin geometries by varying rotational speeds.

Fig. 3.8: During FSP of HEA

3.6 Temperature measurement during FSP

The pyrometer is attached to the FSP machine to capture the temperature distribution during FSP. The temperature data is captured and analyzed by LabView software with the help of a data acquisition system attached to the computer

Fig. 3.9 Pyrometer attached to FSP Machine

Chapter 4

Finite Element Modelling of FSP

Only a little research has been done on high entropy alloys' metallurgical & mechanical properties utilising friction stir processing (FSP). Most of the studies are carried out on experimental work. Some simplified numerical models have also been developed to analyze the temperature distribution and residual stress, which may be connected to microstructure, and to optimize the process parameters of the FSP for other alloys. The numerical modeling method is one of the best methods proven to predict and understand a process, especially when complex and new.

Finite element modeling of FSP is a complex temperature-dependent mechanical process as it mainly involves excessive deformation and a lot of plastic strain and heat. The process parameters like plunge rate, pin length, tool geometries, and rotational and transverse speeds are critical factors in heat and stress generation. The amount of heat produced affects the temperature distribution of the processed specimen. Hence, to obtain a well-processed zone, the combination of process parameters must be optimized, which is critical. Since performing the experiments for different permutations of process parameters becomes a highly tedious and expensive process, a numerical model is created to study the impact of various process parameters on the plate (workpiece).

This research work attempts to understand the complex phenomena involved in FSP. Various modeling studies [42-46] have been tried so far. However, FE modeling of the FSP process is still in its infant stage and requires much more understanding of the complex process to be modeled. The primary focus of the study of finite element modeled FSP is to analyze temperature distribution, stress generated, material deformation, and optimize the process parameters like rotational and transverse speeds to obtain a well-processed zone. A FE model has been developed in ABAQUS CAE to analyse the impact of tool probe geometry, rotational and transverse speeds on the material flow behavior [54]. The experimental data is used to validate the FEM results. The presented findings are preliminary and have to be improvised further.

4.1 Methodology

FEM is a numerical method used to obtain an approximate solution for real-world problems provided with load and boundary conditions. Initially, these problems are represented in complex partial differential equations, which are challenging to solve. In FEM studies, The entire domain is divided into several small elements to reduce the complexity. FEM converts the complex PDEs into a simple system of linear equations(AX=B). The basic steps followed in the FEM process are represented in the figure below:

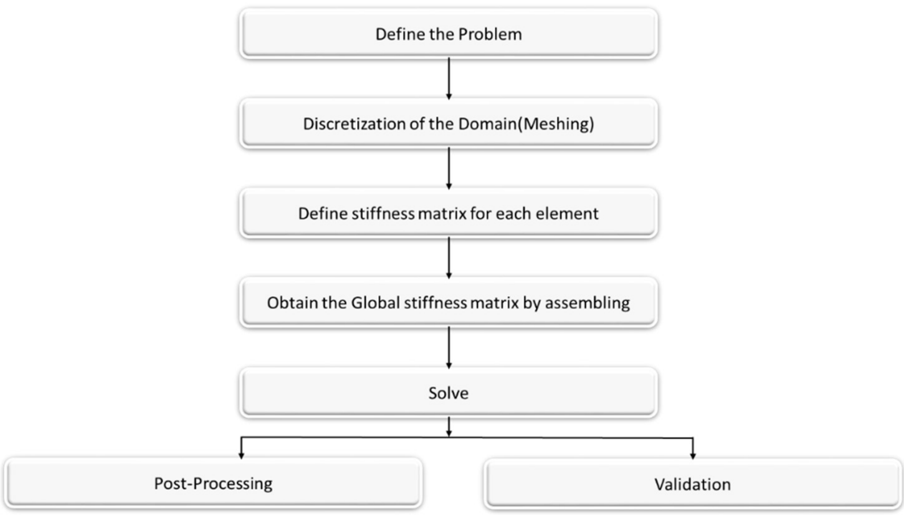

Fig.4.1: Basic steps in the FEM process

ABAQUS/CAE is one of the widely used commercial FEM software. It has many capabilities to analyze problems like simple, linear, complex static, nonlinear, and transient dynamic analysis.

Applications:

The few popular industrial applications of ABAQUS are Automotive Industry, Aerospace Industry, Industrial products industries, Academic research work, and many more.

The finite element model simulation of any problem in ABAQUS mainly consists of 3 different stages. They are:

- Pre-Processing
- ABAQUS Solver
- Post-processing

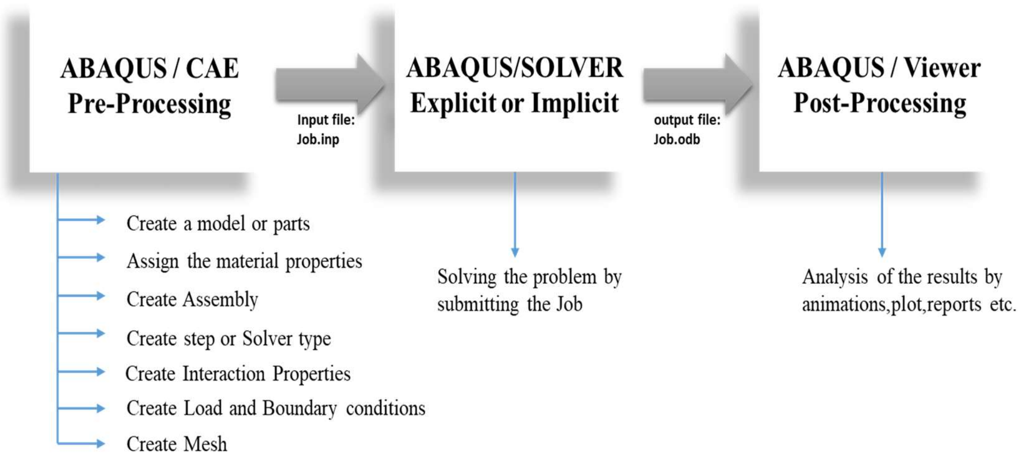

Fig.4.2: Stages in FEM to solve any problems

4.2 Types of Techniques

The types of techniques used for analysis in ABAQUS are classified as follows:

4.2.1 Lagrangian analysis

In the traditional Lagrangian technique, the mesh is coupled to the material points, & the mesh deforms when the material deforms. The Lagrangian elements are always made of the same material. Hence, material and element boundaries coincide. The mesh does not have any corresponding material flow. Therefore, as the material deforms, the node positions will vary, and as a result, the mesh is expected to deform.

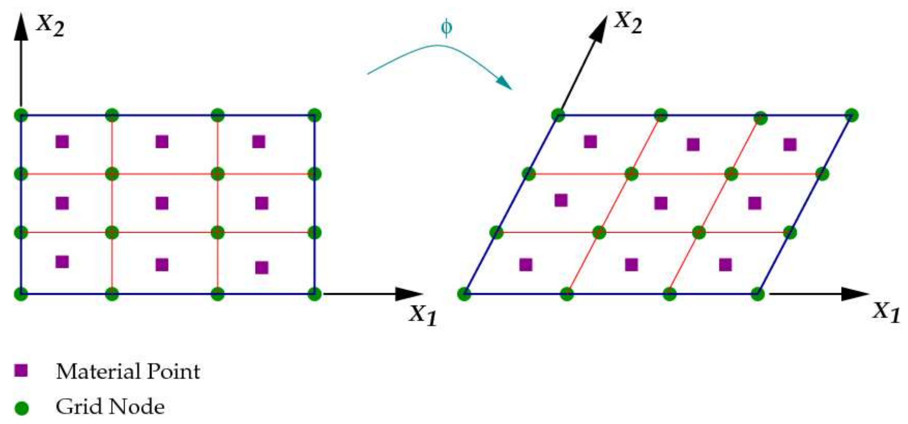

Fig. 4.3: Lagrangian Mesh

4.2.2 Eularian analysis

In contrast to the Lagrangian technique, the Eulerian mesh acts as a background grid in space instead of material, and the material flows through elements that don't deform. The extent of deformation is evaluated when material flows across an element node. In simple terms, mesh deforms in Lagrangian but not in Eulerian. Eulerian elements might be partially or entirely void. This technique allows the material to flow between the elements, and hence, mesh doesn't deform even if the material deforms. If material leaves the Eulerian mesh, it is deemed completely lost from the study.

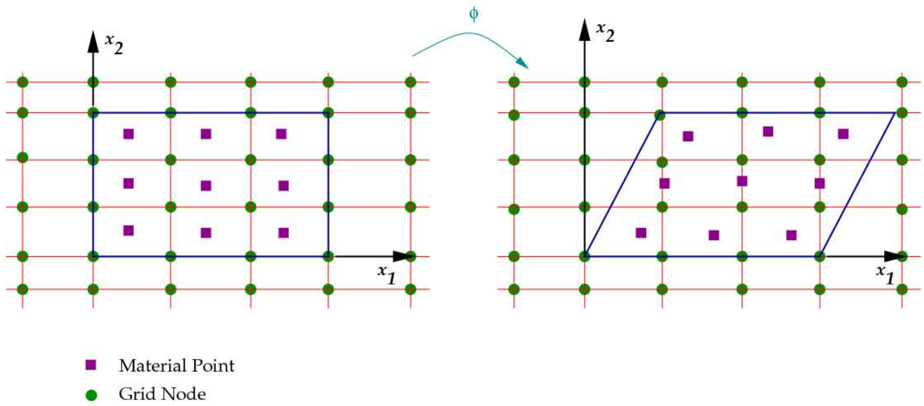

Fig. 4.4: Eulerian Mesh

4.2.3 Coupled Eulerian-Lagrangian (CEL) technique

Another technique that has attracted significant attention in FE modeling is the Coupled Eulerian-Lagrangian (CEL) analysis. This technique combines both Lagrangian and Eulerian techniques in the same analysis. The primary purpose of this technique is to avoid mesh problems while simulating excessive deformations processes. The most commonly used technique in FE analysis is the Lagrangian technique, but it is not suitable for the operation where excessive deformation is expected. In those cases, the Eulerian technique is predominantly applicable. The CEL technique enables to mesh of the components selectively, i.e., The Eulerian meshing technique is used for the components which undergo excessive deformation, while the others are meshed using the Lagrangian approach. The present work uses the CEL technique as the workpiece undergoes excessive deformation in FSP.

4.3 Pre-Processing:

The Pre-processing stage is also known as ABAQUS/CAE modeling stage. This stage entails defining the engineer's proposed methodology of the physical problem by creating load and boundary conditions. This CAE file is called as ABAQUS input file. The model can either be built-in graphically using ABAQUS/CAE or imported from any other CAD software.

4.3.1 Building a Model / Geometry

Developing a Geometry stage requires more time than any other stage of FEM analysis of any problem based on complexity. First, select the new model database with the ABAQUS standard/Explicit model to create parts and save the CAE file. Right-click the parts section &select Create. The geometry of the workpiece and tool are created as per the requirement. The below figures illustrates the tool and workpiece being designed.

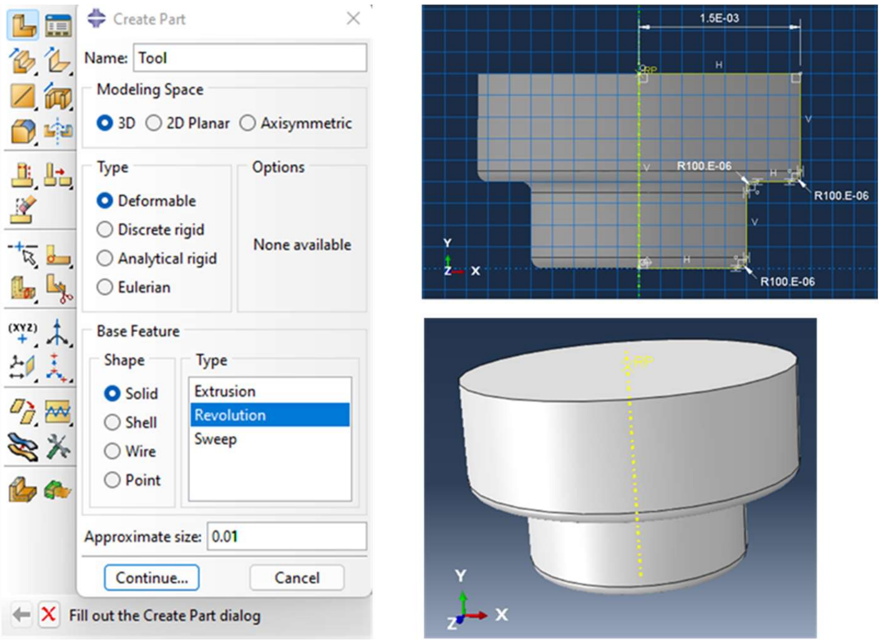

Fig. 4.5: Tool Design in ABAQUS

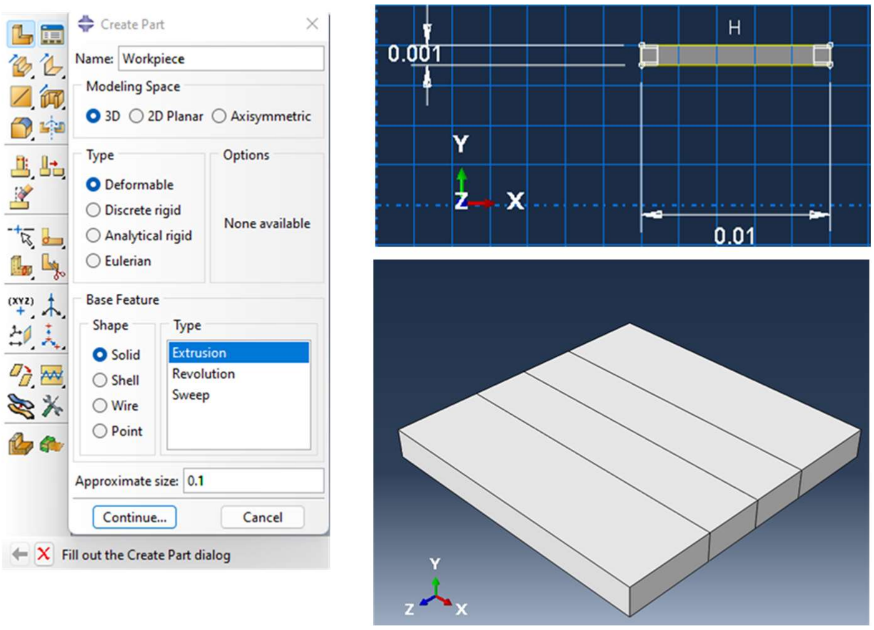

Fig.4.6: Workpiece (Lagrangian) Design in ABAQUS

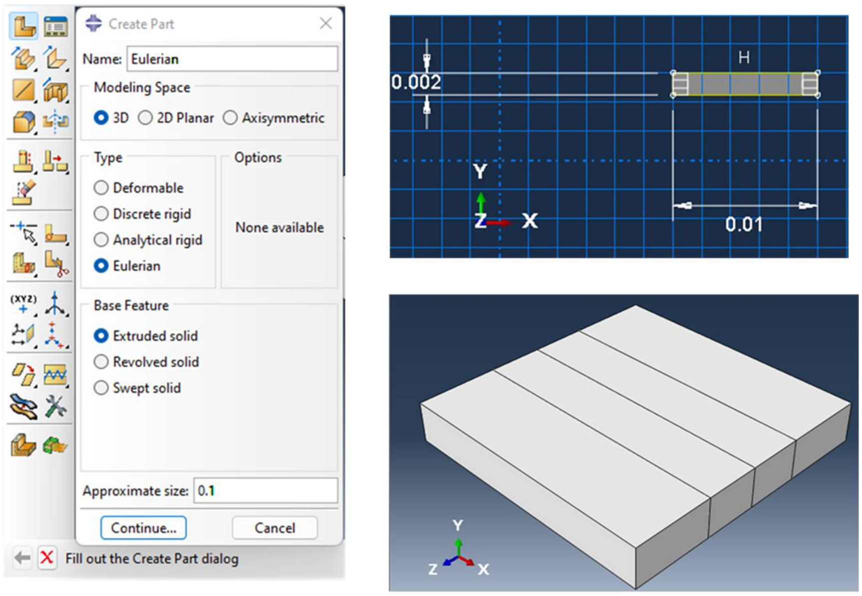

Fig.4.7: Workpiece (Eulerian) Design in ABAQUS

4.3.2 Material Definition

In the Property module, create new material and input all the properties required for the simulation in corresponding sections.

The following material properties are considered in the simulation

Material Property	HEA alloy - Work piece	WC - Tool
Density	7860 kg/m^3	11900 kg/m^3
Thermal Conductivity	5.989 W/m-K	50 W/m-K
Specific Heat	460 J/Kg-K	400 J/Kg-K
Young's Modulus	205 GPa	534 GPa
Poison's ratio	0.29	0.22
Expansion Co-efficient	1.65 e^-05 1/K	

Table. 4.1: Material properties used for Simulation

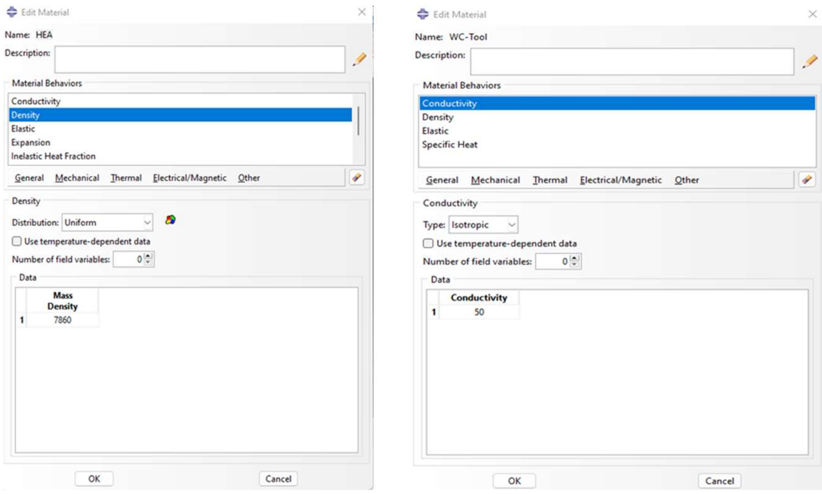

Fig. 4.8: Material Definition – Edit material window of HEA Workpiece and WC Tool

4.3.2.1 Plasticity material model:

In the processes like FSP, the workpiece undergoes excessive deformation and continuous change in temperature throughout the process. Hence, it is essential to consider the material softening effect due to the heat produced by friction between the plate and the tool. The literature shows that the Johnson-Cook material model [8,10,11] considers the thermal softening effect. The present research uses the Johnson-cook model to assess plastic deformation. It shows how flow stress changes with plastic strain, plastic strain rate, and temperature. This phenomenological model is mainly for excessive deformation processes. It considers an extensive range of strain rates and temperature changes that are relevant to large plastic deformation due to thermal softening. This mathematical equation assumes strain-hardening, strain rate-hardening, and thermal softening.

The Johnson-Cook equation is as follows:

$$\sigma = \underbrace{(A+B\,\varepsilon^{n})}_{\text{Strain Hardening}}\underbrace{\left[1+C\ln\left(\frac{\dot{\varepsilon}}{\dot{\varepsilon}_{o}}\right)\right]}_{\text{Strain rate Hardening}}\underbrace{\left[1-\left(\frac{T-T_{ref}}{T_{Mp}-T_{ref}}\right)^{m}\right]}_{\text{Thermal Softening}}$$

Where,

σ = Material's Flow stress A = Yield stress at zero strain (MPa)

ε = Plastic strain B = Hardening modulus (MPa)

n = Exponent of Strain Hardening

C = Strain rate coefficient $\dot{\varepsilon}$ = Plastic strain rate

T = Instantaneous temperature $\dot{\varepsilon}_{o}$ = Reference strain rate ($10^{-4}\,s^{-1}$)

T_{ref} = Reference/Transition temperature

The Johnson-cook equation model parameters utilized in the current research can be seen in the table.

A	B	n	C	m	T_{Mp}	T_{ref}
216 MPa	1000 MPa	1.2	0.145	0.01	1808 K	293 K

Table. 4.2: JC Parameters used for Simulation

To assign the material properties to the parts, create sections and assign the sections to the respective regions. Double-click on the sections and later section assignments in the Model tree.

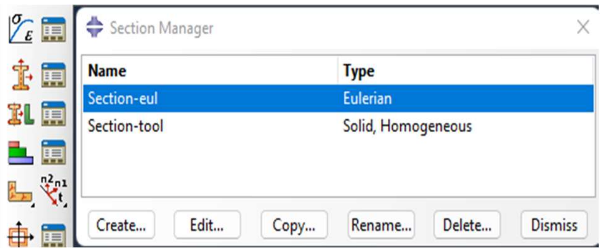

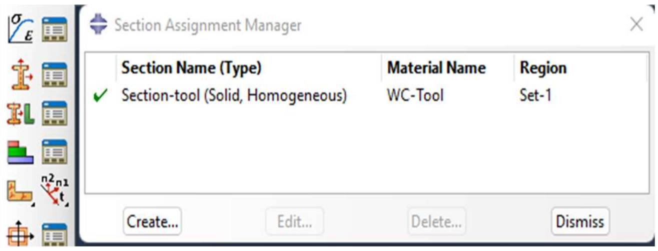

Fig. 4.9: Creation & Assignment of sections

4.3.3 Assembly of Parts

Assemble the parts under the assembly section by double-clicking on the instances in the Model Tree. The Lagrangian plate is placed inside the Eulerian container by coincident point constraint.

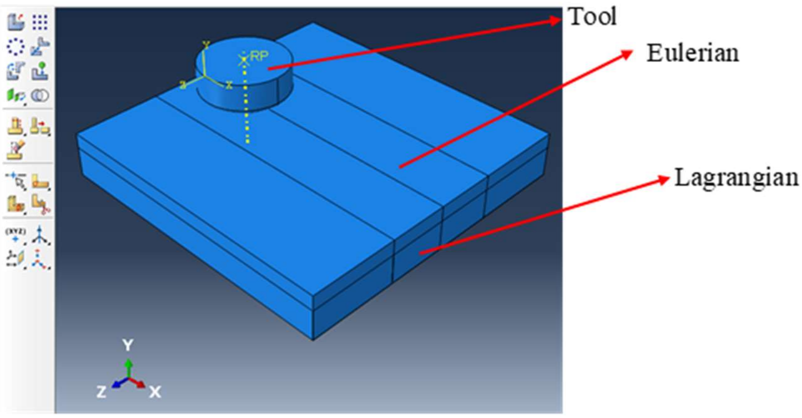

Fig.4.10: Assembly of the workpiece and tool for FSP

4.3.4 Definition of steps

Generally, FSP involves three Phases. They are Plunging, Dwelling, and Processing. The dwelling stage is ignored to reduce the computational time and cost, and the other two phases are created in the step manager. Finite element modeling involves solving complex nonlinear equations. The set of equations to be solved, availability of specific features, and run duration are all influenced by the type of solver utilized. The solvers in FEA represent the type of algorithm used for time incrementation. In both solvers, the model's state is calculated at various points in step time, and the new state is calculated based on the data available at the old state.

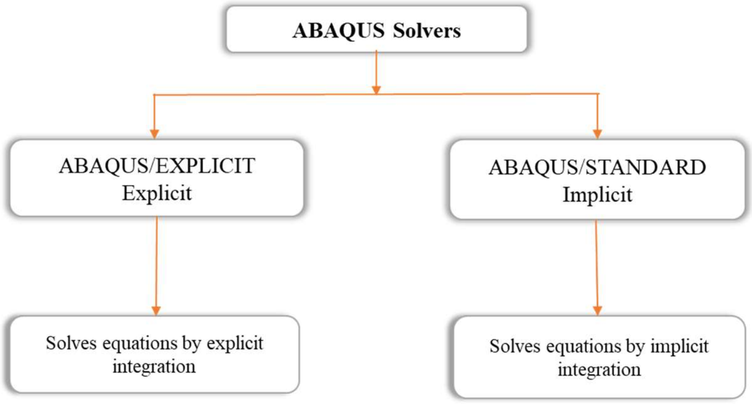

Fig.4.11: Solver Types in ABAQUS

ABAQUS/EXPLICIT Explicit solver :

In the ABAQUS explicit algorithm, the new state or position is directly calculated from the data available in the current state. Typically it is an extrapolation. The larger time increments lead to more significant errors in the solution.

ABAQUS/STANDARD Implicit solver :

The new state cannot be directly calculated from the old state; a coupled system of equations typically uses the Newton-Raphson method must be solved. The larger time increments do not lead to more large errors in solutions due to the iterative approach used (Newton-Raphson method).

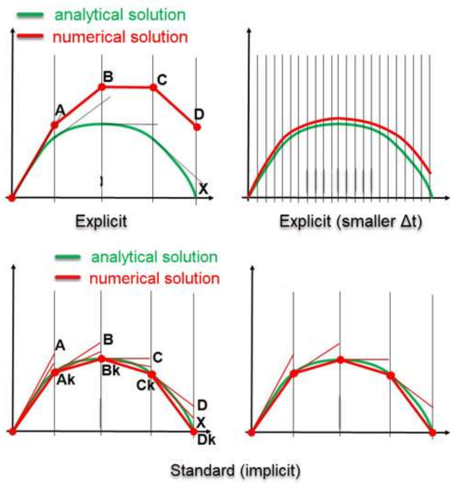

Fig.4.12: Time incrementation with Explicit and Implicit (Standard) solver

Therefore, choosing between Explicit and Implicit solvers is often choosing between many small increments and fewer larger increments.

The main differences between Implicit and Explicit solvers are:

EXPLICIT SOLVER	IMPLICIT SOLVER
Small computational cost per increment	High computational cost per increment
Small-time increments	Large time increments
Approximately constant stable time increment size	Strongly varying increment size for nonlinear problems
Dynamic problems	Static or Dynamic problems
CEL is applicable	CEL is not applicable

Table 4.3: Explicit Solver Vs. Implicit Solver

4.3.4.1 Dynamic explicit solver

A dynamic explicit solver is one of the most widely used solvers for both linear and nonlinear problems in ABAQUS due to its versatility. Nonlinear problems involve many highly complex calculations, which increases computational costs. In any problem, non-linearities arise due to the following:

a) cross-section's geometric non-linearity
b) Material non-linearity
c) Load and Boundary conditions non-linearity.

In the current research, a dynamic,temperature-displacement explicit solver is used. It considers the effects of both thermal and mechanical. The 'Dynamic, temperature- displacement, explicit solver is specifically used for highly nonlinear processes in which elements are excessively deformed. The explicit algorithm handles these large deformations and is computationally expensive.

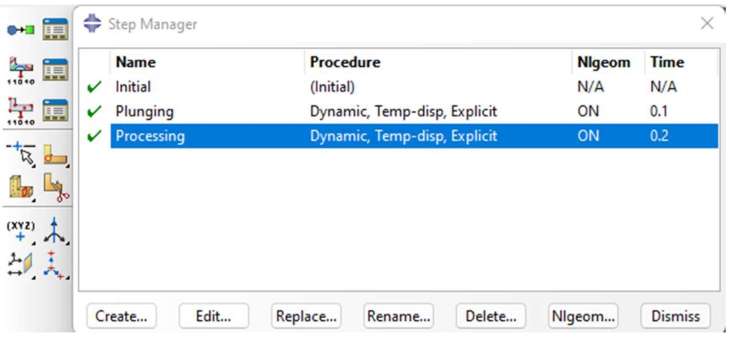

Fig. 4.13: Step Manager

4.3.4.2 Time incrementation and simulation stability

A stable time incrementation is a time required for each increment in step time. In ABAQUS, there are two primary methods of time incrementation. They are as follows:

a) Fixed time incrementation method
b) Automatic time incrementation method.

The static or fixed time incrementation method takes manually fed user input and uses it throughout the simulation. However, this method has a few drawbacks, and the results may not be accurate for excessive deformation problems. On the other hand, the system calculates the stable time increment for the analysis and uses it throughout the simulation in an automatic method.

In the automatic method, the value of the stable-time increment is obtained using the following method

$$\mathbf{\Delta T < \min(L_e/C_d)} \tag{3}$$

Where L_e = Element's characteristic length and C_d = speed of sound in the material medium. The minimal value of Le and C_d ratio of all elements of the component is referred as stable-time increment. Further, C_d is computed as follows:

$$\mathbf{C_d} = \sqrt{E/\rho} \tag{4}$$

Where,

E = Modulus of Elasticity and **ρ** = material density.

The time increment always must be conditionally stable in the simulation of any problem in ABAQUS. ABAQUS always picks a value less than the minimal value of Le and Cd ratio when the automatic time increment is selected. Whereas in the fixed time increment method, value is considered with utmost care; otherwise, the simulation will terminate if the value crosses the stability limit.

The essential points to remember about stable time incrementation are: -

a) The size of the minor element limits stable time increment. Hence, finer mesh takes a long time to converge due to lower time increment.
b) As Young's modulus increases, the time increment reduces.
c) As the density of the material increases, the time increment rises.

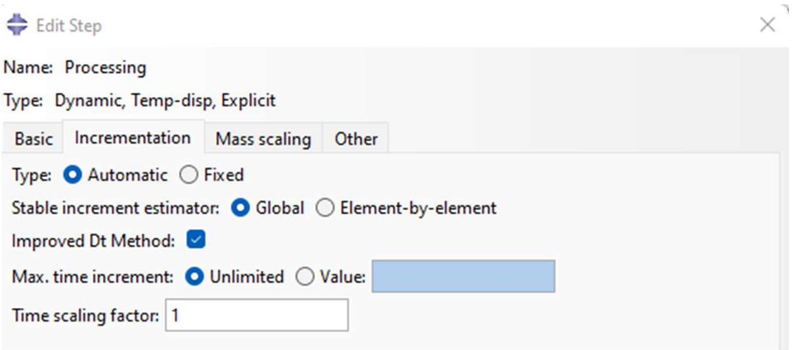

Fig. 4.14 Window to choose fixed or automatic time increment

4.3.4.3 Methods to reduce analysis time

ABAQUS is a potential tool to simulate any complex problem with various material contact behaviors like high strain rate deformation, quasi-static material behavior, fluid flow, and many complex multiphysics material problems. Any problem to be solved in ABAQUS is generally classified as either an Explicit or Implicit problem. The problems involving high strain rate deformations, thermo-mechanical studies, excessive deformation, and explosive material behaviors are usually solved using an explicit method. These problems are generally dynamic and involve solving many mathematical equations in the backend to replicate the material and other parameter behaviors.

These dynamic problems are computationally expensive; it may take numerous hours to solve even 1 second step time in ABAQUS due to the associated complexities in the analysis. So to reduce the simulation time without any change in results, ABAQUS allows accelerating the simulation through scaling methods.

The simulation can be accelerated by following scaling methods:

a) Mass scaling
b) Time scaling
c) Parallelization

Mass scaling

Based on equation (1), ABAQUS calculates the stable time incrementation for simulation of any problem. The stable time increment value depends on the minimal value of the ratio of L_e and C_d of all the elements. Stable time increment is extremely low in most explicit problems, so a model's computational cost is high. From equation (1), the stable-time increment is directly related to the square root of the density of the material. Therefore, lighter materials would result in tiny time increments. Hence, simulation time is significant when compared to heavier materials. In ABAQUS, mass scaling allows the user to manipulate the density (and therefore the mass) by a specific factor. The mass scaling factor may be either set manually or automatically. The stable time increment increases by root over its scaling factor by mass scaling. In return, it reduces the computational time and cost.

Time scaling

Many researchers have also tried the time scaling method to decrease the computational cost and time. In this method, the total time spent on the analysis is lowered to a much smaller value. The input parameters such as plunge rate, rotating & traversal speeds should also be increased by the same factor to obtain accurate results. Although this method effectively reduces the computational cost, care must be taken to prevent the dynamic effects of the material properties that may be rate-dependent.

Parallelization

The parallelization process is a hardware-dependent method to reduce the computational cost. ABAQUS allows users to utilize multiple cores for solving an explicit problem which may take longer while using a single core. As the number of cores increases, the simulation time reduces.

4.3.5 Definition of Interaction Properties

In FSP, the friction between the plate and tool is the principal cause of heat generated. Schmidt et al. constructed an analytical equation that describes the heat produced at the tool's shoulder by both sticking and sliding friction [7]. According to this equation, the bottom surface of the shoulder and pin's contact surface generate over 90% of the heat. Thus, the heat equation that represents the primary heat source is

$$\rho C \frac{\partial T}{\partial t} = Q + \frac{\partial}{\partial x}\left[K_x \frac{\partial T}{\partial x}\right] + \frac{\partial}{\partial y}\left[K_y \frac{\partial T}{\partial y}\right] + \frac{\partial}{\partial z}\left[K_z \frac{\partial T}{\partial z}\right] \qquad \text{(a)}$$

Where,

ρ = material density	T = Temperature
C = Specific heat	K = Thermal conductivity in three directions
Q = Heat generated	t = elapsed time

The literature shows that the heat required for FSP is generated due to Coulomb's frictional heat and plastic deformation [29,42,43]. The frictional heat generated is the function of the normal force acting on the workpiece and the tool's rotational speed. The equation is written as

$$Q_f = \mu 2\pi R N F_n \qquad (2)$$

Where,

μ = coefficient of friction	R = point from the tool centre
N = tool rpm	Fn = Normal force

The heat produced due to plastic deformation is written as

$$Q_p = \eta \tau \dot{\varepsilon} \tag{3}$$

Where,

η = fraction of heat dissipated due to plastic deformation,

τ = shear stress $\dot{\varepsilon}$ = plastic strain rate.

Salloomi et al. [43] suggested that heat produced due to plastic deformation is lower than 10% of the overall heat generated. Therefore, it is clear that the friction between the plate and the tool shoulder generates a large quantity of heat.

In the ABAQUS, the general contact is specified between the plate and the tool of the FSP. The slipping condition is assumed between them, and the maximum slip value used is 0.5% which is the default value. In the interaction property manager, contact between the plate and tool is specified in the plate's tangential and normal directions. Hard contact is specified in a normal direction, & penalty contact is utilised tangentially. From the literature, the recommended friction coefficient is 0.3-0.4 [14]. It is defined that frictional heat generated is distributed uniformly across the plate. In the constraint manager, the tool is specified as a rigid body to simplify things.

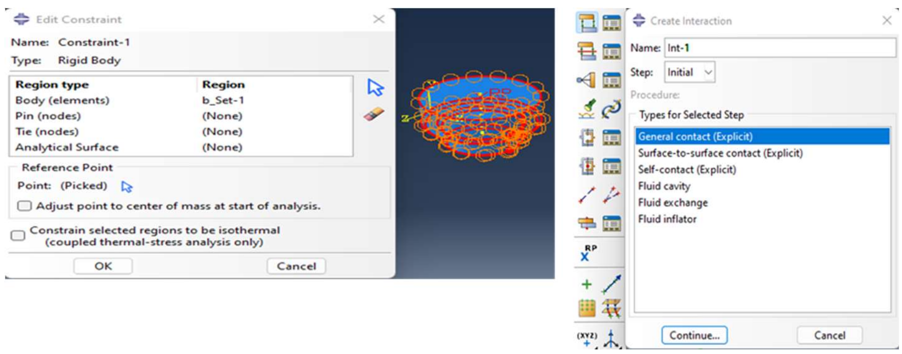

Fig. 4.15: Rigid Body constraint & contact definition

4.3.6 Definition of Loads and Boundary conditions

In the simulation of any problem, loads and boundary conditions play a crucial role. The Boundary conditions should be selected with the utmost care to obtain accurate results. The results depend on the boundary conditions assumed in the model. In the processes like FSP, temperature, heat transfer, and physical constraints are considered for accuracy. The bottom surface of the Eulerian medium is constrained from movement in all directions by applying the encastre boundary condition. In the CEL technique, the eulerian mesh acts rigidly. Thus, velocity constraints are used on the boundaries of the eulerian medium to avoid material escaping from the faces. The tool's plunging, rotational, and transverse speeds are applied to the reference point specified. The current study assigns the tool's rotating speeds of 800 & 1000 rpm. The fixed traversal speed of 20 mm/min and a 5 mm/sec plunge rate is set to tool in the processing direction. A pre-defined temperature field is assigned to both the workpiece and the tool to room temperature, i.e., the tool and workpiece are assumed to be at ambient temperature before the beginning of FSP. The current study divides FSP process into two steps. They are plunging and processing. Plunge rate and rotational speed are assigned to the reference point during the plunging stage. During the processing stage, rotational and transverse speeds are provided.

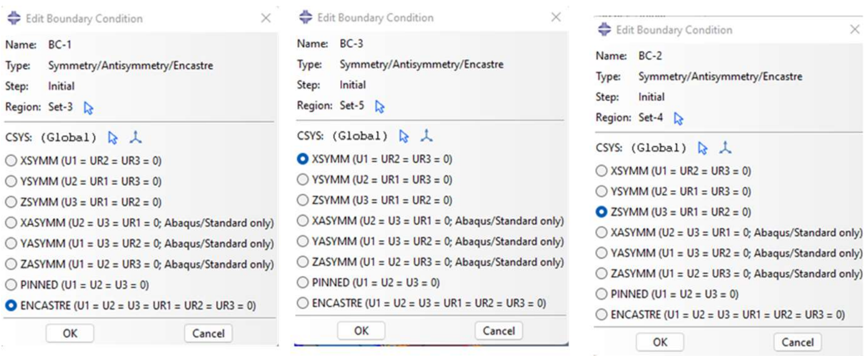

Fig. 4.16: Boundary Conditions

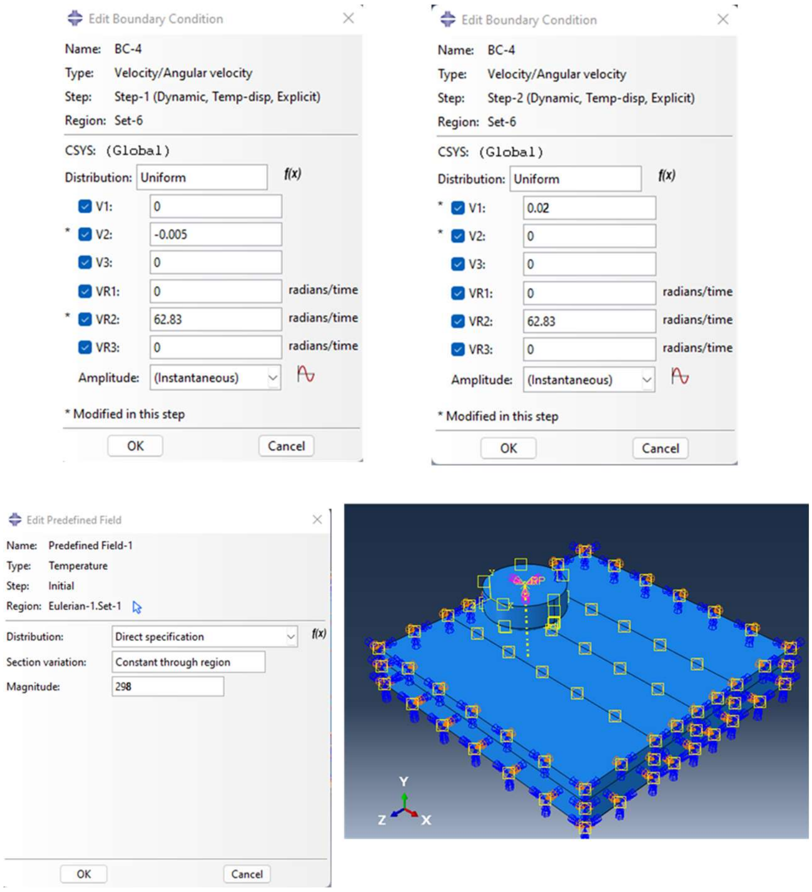

Fig.4.17: Load conditions and pre-defined field

4.3.7 Definition of Mesh

In any Finite element simulation, the entire domain is discretized into numerous small elements. This discretization is called meshing. Meshing is a fundamental step in every simulation. Hence, it plays a crucial role. Mesh quality defines the accuracy of the results and computational cost. It is essential to keep an eye on the number of elements obtained after discretization—computational cost increases as the number of elements increases, i.e., very finer mesh. If the coarse mesh is used, the results may not be accurate. So, it is imperative to optimize the mesh size. Mesh depends on the complexity of geometry.

In the current work, the Eulerian medium has meshed with 19,116 multi-material 8-node thermally-coupled linear eulerian-brick, hourglass control, and reduced integration (EC3D8RT) elements. Each element has 4 degrees of freedom at every node. The Bias meshing technique is used to produce a finer mesh in the processing area & a coarse mesh in the other area to improve computational efficiency. The element uses both reduced integration and hourglass control techniques. The element shape is similar to the BCC unit cell containing nodes at the center and eight corners.

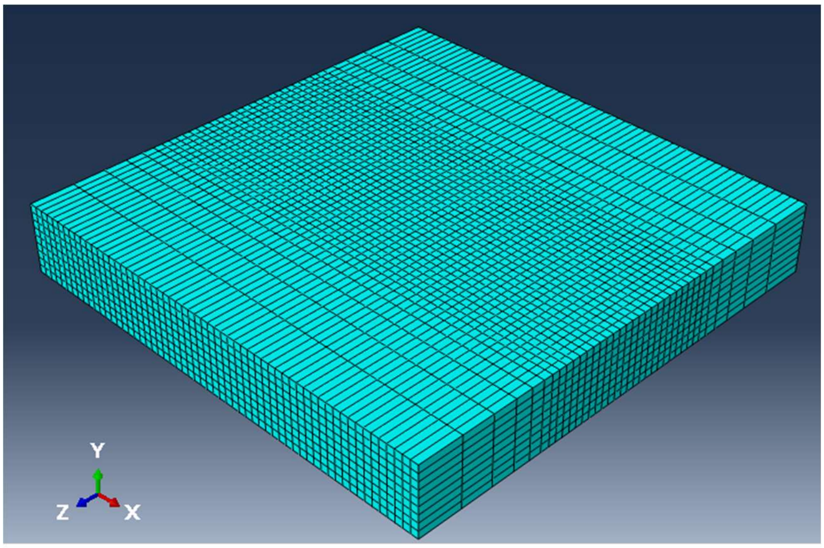

Fig.4.18: Meshing of an Eulerian Part

The Lagrangian tool has meshed with 5957 4-node thermally-coupled tetrahedron, linear displacement, and temperature (C3D4T) elements

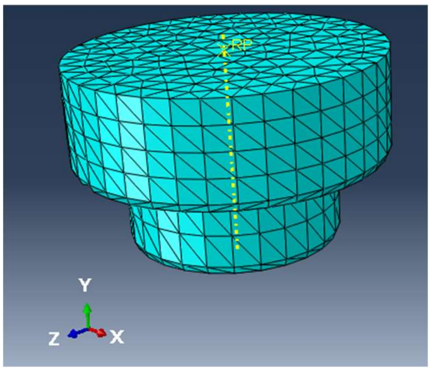

Fig.4.19: Meshing of a Tool

It is not required to mesh the Lagrangian plate. The volume fraction of the eulerian meshed part is calculated. In the conventional Lagrangian approach, the part is meshed, whereas in the CEL approach, the eulerian part has meshed, and the Lagrangian part is placed in the eulerian part. The material flows into the eulerian mesh as it deforms.

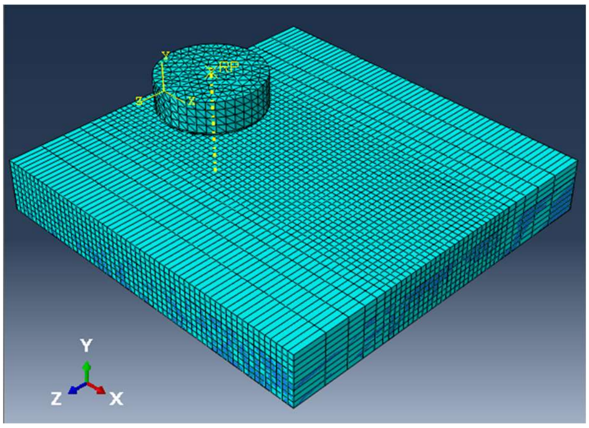

Fig.4.20: Assembly view after meshing

4.4 Abaqus solver:

In pre-processing, the created or imported input file is submitted for analysis and starts solving for results in this stage. Abaqus uses ABAQUS/Explicit or ABAQUS/Implicit to solve the problem based on the user selection. Based on the complexity of the problem and the computer's specifications, the simulation time may range from seconds to days. In the current study, ABAQUS/Explicit solver is used to solve the problem. The job is created and submitted for analysis in this stage for results.

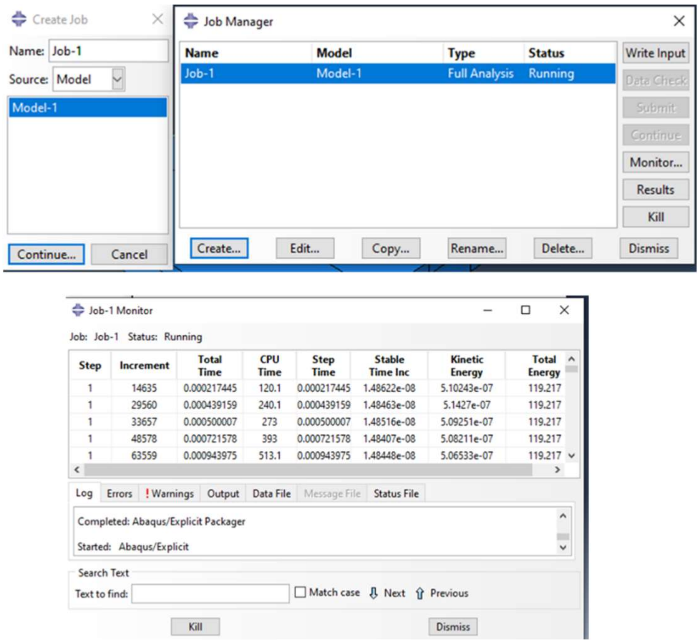

Fig.4.21:Job submitted monitoring section

4.5 Post-processing:

In this stage, the obtained results are evaluated by contour plots, graphs, animations, reports, etc., after the simulation is completed. The post-processing can be done either by ABAQUS/Viewer or any other postprocessor.

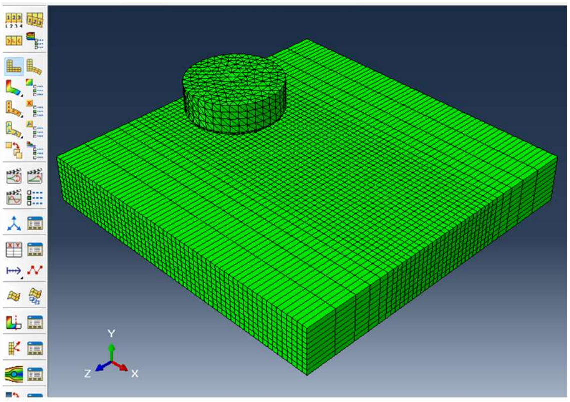

Fig.4.22: Post-processing window

Chapter 5

Results and Discussion

5.1 Metallographic Analysis:

The heat due to friction between the plate and the tool softens the material. Due to the force of the shoulder and the stirring effect of the pin, the softened material undergoes additional plastic deformation and recrystallization. As a result, the FSPed zone achieves a fine and homogeneous microstructure. After FSP, four different regions were discovered based on the microstructural examination of grain sizes, and they are as follows:

- Stirring Zone (SZ)
- Thermo-mechanically affected zone (TMAZ)
- Heat Affected Zone (HAZ)
- Base metal zone (BM)

Microstructural variations in different regions have a significant impact on the mechanical characteristics of the FSPed zone. The following figure depicts the formation of different zones:

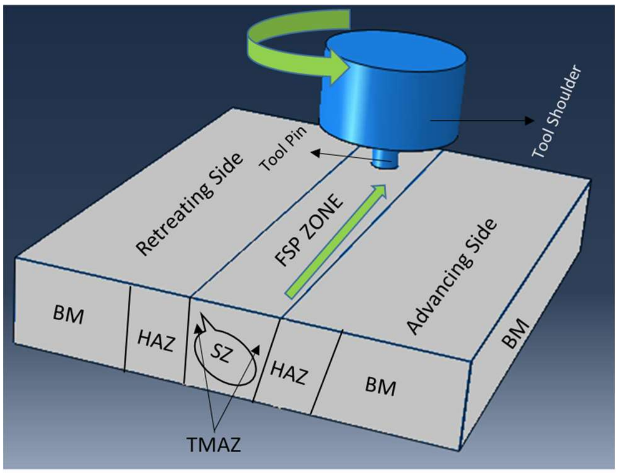

Fig.5.1: Formation of different zones after FSP

The microstructure of both as-received and FSPed samples of $Al_{0.3}CoCrFeNi$ HEA is observed using Scanning Electron Microscopy (SEM). The HEA samples FSPed at different tool rotational speeds with two-pin profiles (square and circular cross-section) are sliced along the cross-sectional area and prepared for the metallographic investigation. The findings show that the grain size of untreated HEA is around 40 μm, and significant grain refinement is noticed in the stirring zone post-FSP.
The following figures depict the Scanning Electron Microscopy images of the grains in different zones

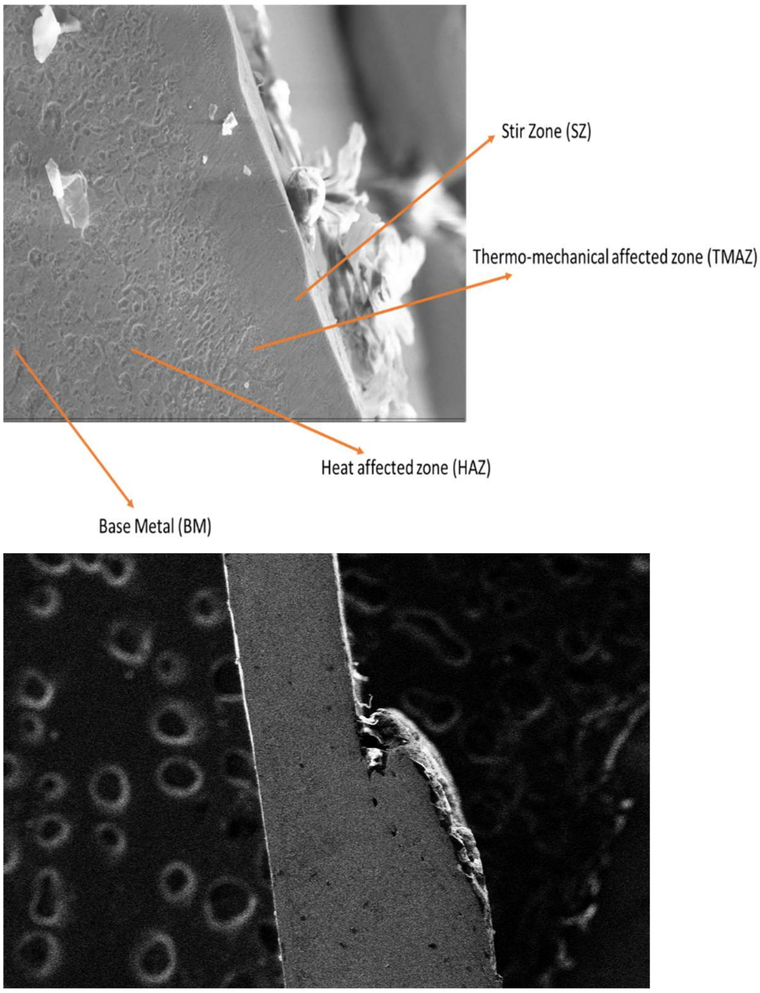

Fig.5.2 SEM image of the different zones

From the figure, it is clear that different grain sizes are observed in distinct zones. The grain size increases from the stirring zone (SZ) to the Base Metal (BM). Very fine grains are observed in the stirring zone.

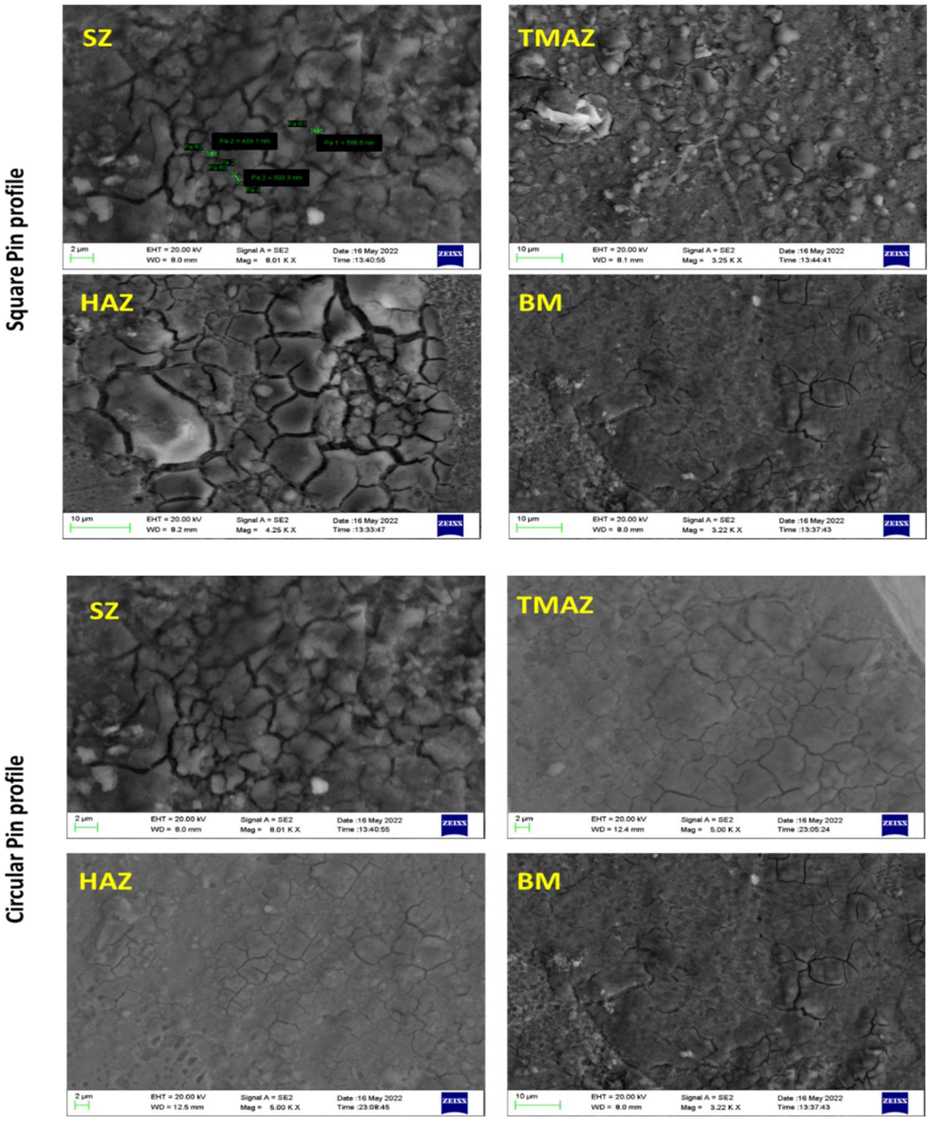

Fig.5.3: SEM images of Grain size in different zones

In the current study, the square probe profiled tool produced a defect-free processing zone compared to the cylindrical profile. The grain size in the stirring is reduced from micron level to nano levels. The square pin profile had more refined grains than the cylindrical pin profile in the stirring zone.

It has been noticed that increasing rotating speed lowers the grain refinement, which is consistent with Sato et al.'s observations [30]. Sato et al. found that grain size grows exponentially with the rise in maximum temperature, which in turn is related to the rise in rotational speed. Therefore, it is clear that the frictional heat increases as the rotating speed increases.

This increases peak temperature in the FSPed zone, which leads to grain growth. Although there was significant grain refining at each speed, the grain size rose as the rotating speed was increased, resulting in equiaxed and uniform grains.

5.2 EDS Analysis:

The elemental composition was determined using Energy Dispersive X-ray Spectroscopy at several places across the stir zone. The below figures depict two selected areas, spectrum 6 & spectrum 7 of the FSPed region by square pin profile and circular pin profiled tools, respectively, where the elemental composition is obtained.

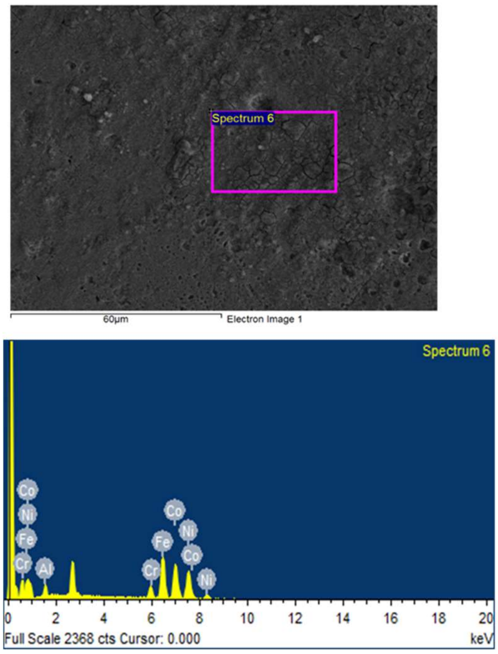

Element	Atomic%
Al K	6.22
Ni K	23.33
Cr K	23.30
Fe K	24.42
Co K	22.65
Totals	100

Fig.5.4: EDS analysis of FSPed region using square pin profile

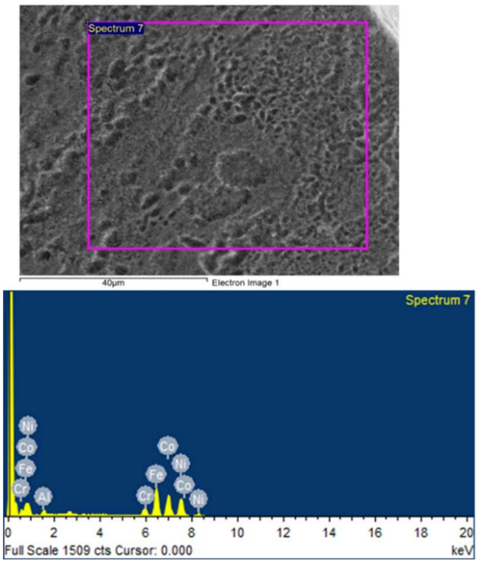

Element	Atomic%
Al K	8.62
Ni K	22.83
Cr K	22.90
Fe K	23.40
Co K	22.25
Totals	100

Fig.5.5: EDS analysis of FSPed region circular pin profile

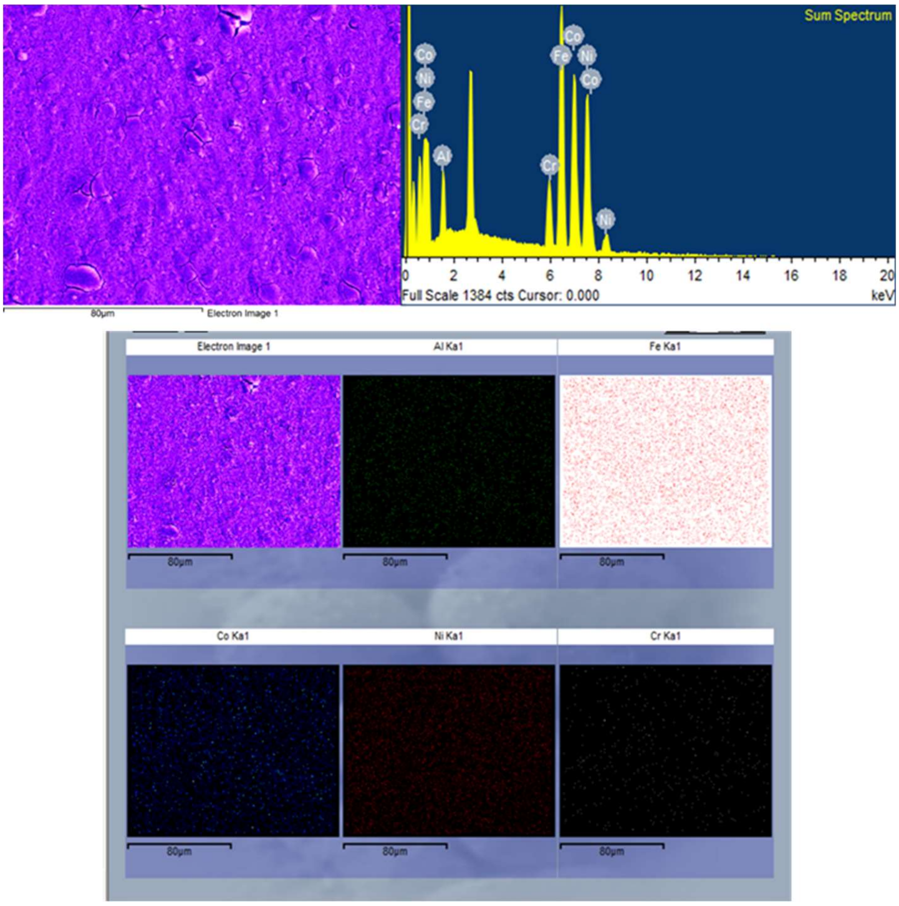

Fig.5.6 Area Mapping of the elemental composition of $Al_{0.3}CoCrFeNi$ HEA

The analysis shows that $Al_{0.3}CoCrFeNi$ HEA has a nearly equimolar composition of Co, Cr, Fe, Ni, and aluminium as a minor elements.

5.3 XRD Analysis:

Both as-received and FSPed samples are subjected to XRD examination. All the peaks are identified and indexed using Xpert Highscore software from the obtained plots. From the XRD pattern, only the FCC phase is detected in both as-received and FSPed samples. Ignoring certain minor picks, only three significant peaks are identified in the XRD pattern of $Al_{0.3}CoCrFeNi$ HEA. The obtained XRD patterns are consistent with the literature.

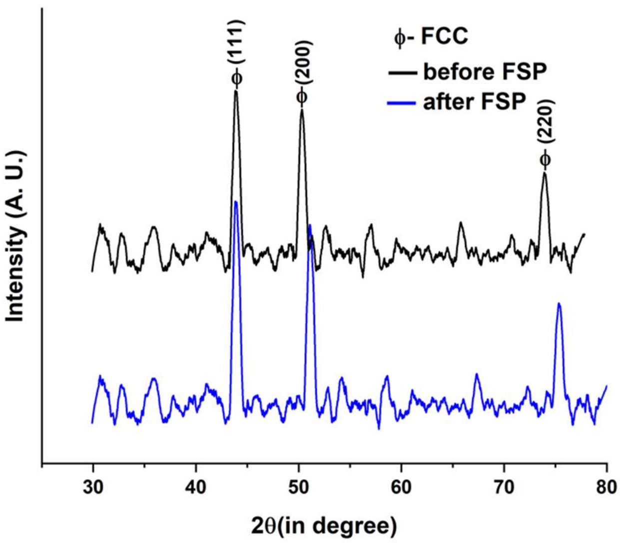

Fig.5.7: XRD Patterns of $Al_{0.3}CoCrFeNi$ HEA before and after FSP

5.4 Micro-Hardness Investigation:

Vickers micro-hardness distribution is evaluated across the cross-sectional area of samples in various zones. The micro-hardness test is performed on four samples: square pin profiled (800 & 1000 rpm) and circular pin profiled (800 & 1000 rpm) tools. The following figure depicts the micro-hardness profile of four processing conditions:

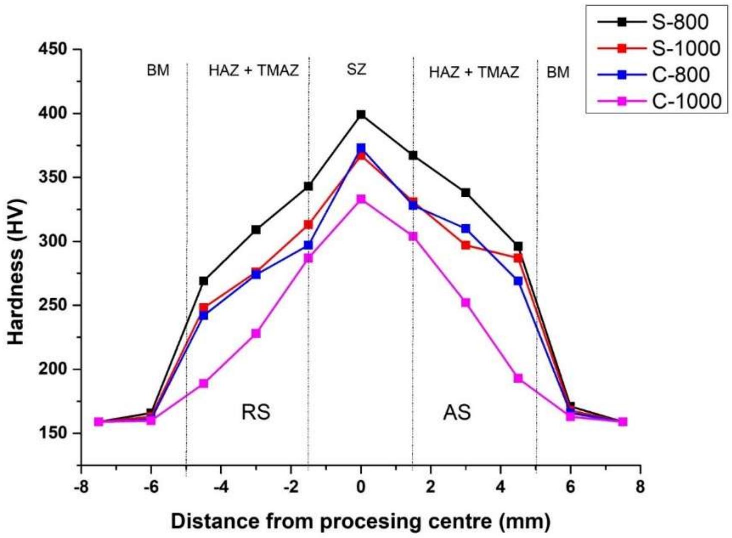

Fig.5.8: Micro-hardness distribution profile of FSPed samples

The hardness distribution pattern shows that the highest hardness is noticed in the stir zone's centre. The drop in hardness at the HAZ is because there is no mechanical deformation (stirring) in that region, yet, the maximum temperature attained softens the material adjacent to the processed area.

Pin geometry has a significant impact on the material flow behaviour. The pin geometry with flat surfaces/faces like a square pin-profiled tool produces a pulsating stirring phenomenon, whereas cylindrical pin profiles do not have this pulsating phenomenon. Out of all the four processing conditions, the FSPed area produced with S-800 had the maximum hardness of 399 $HV_{0.1}$, whereas the area produced with a C-800 had the lowest hardness value of 334 $HV_{0.1}$.

The graph indicates that the hardness value drops as the rotating speed increases, irrespective of the tool pin profile. This is because as the rotating speed increases, so will the heat input, causing the material to soften more due to grain expansion.

According to the Hall-Petch relationship,

$$H_V = H_o + K_H d^{-1/2}$$

Where, H_o & K_H are constants. The hardness is inversely related to the grain size. Hence, as the rotating speed increases, grain growth increases, and hardness value decreases. Therefore, more grain refinement is accomplished at lower tool rotational speeds.

5.5 Micro-Tensile Testing:

The samples are cut from the as-received and FSPed using two different tool profiles. At room temperature, the tensile samples are subjected to a 1mm/min tensile test speed. The following figure depicts the tensile specimens:

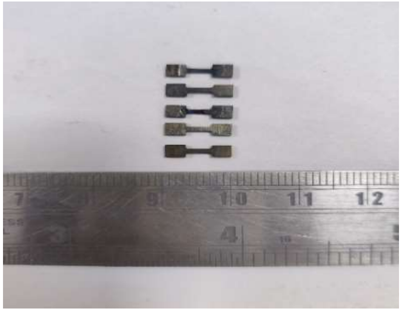

Fig.5.9: Tensile specimens of different processing conditions and base material

Fig.5.10: Fractured samples of tensile tests

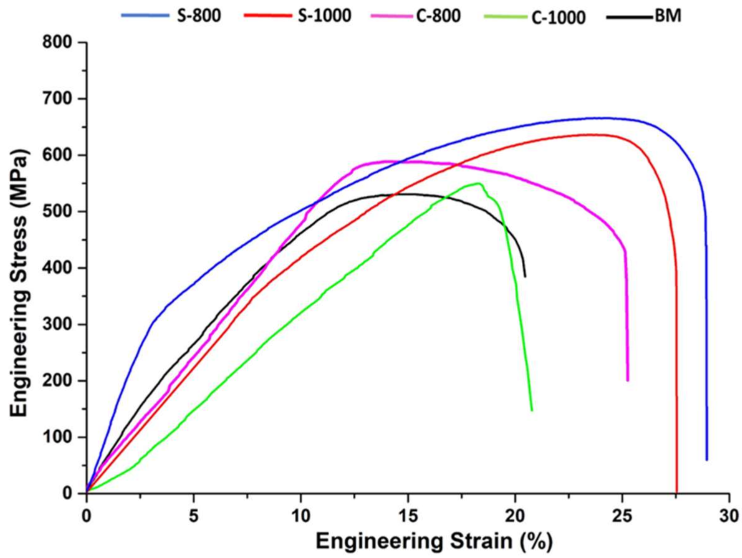

Fig.5.11: Engineering stress Vs. Engineering strain (%)

The graph illustrates that the samples treated with square profiled pin tools had a higher Ultimate Tensile Strength than those processed with cylindrical pin profiled tools. This is due to the fact that a square-pin-shaped tool's stirring zone experiences more pulsing motion. The pulsating action produces excessive turbulence of the plastically deformed material in the stir region, which leads to a more refined microstructure. Thus, the FSPed region using the square-pin profile tool contains more refined grains than the circular-pin profile region. As a result, the FSPed region using the square-pin profiled tool has greater strength and hardness. To illustrate this relationship, Callister [52] presented the Hall-Petch equation:

$$\sigma = \sigma_o + Kd^{-1/2}$$

According to this relation, strength (σ) increases as grain size (d) decreases.

The graph is plotted between the UTS, % of elongation, and Yield strength of each processing condition. It is noticed that the S-800 processing condition produced a processed area with higher values of UTS, YS, and % of elongation relative to the other processing conditions.

The table indicates the UTS, YS, & % of elongation values for each processing condition.

S.No	Sample	% of Elongation	Yield Strength (MPa)	Ultimate Tensile Strength (MPa)
1	BM	20.4	336.5	527.32
2	C-800	24.8	500.571	589.78
3	C-1000	21.3	390.41	549.97
4	S-800	28.7	603.5	665.25
5	S-1000	27.6	550.571	637.67

Table 5.1: UTS, YS, % of Elongation for each processing condition

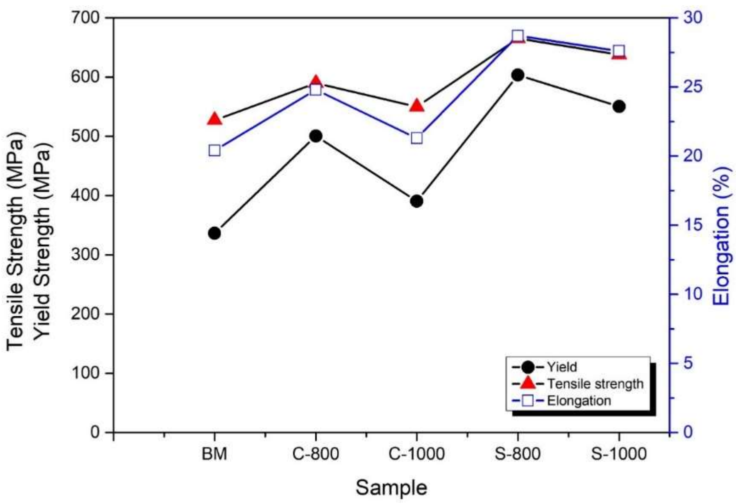

Fig.5.12: UTS, YS, % of Elongation Vs. Processing condition

5.6 Numerical (FEM) Model Analysis:

5.6.1 Temperature Distribution:

The heat generation owing to friction and plastic deformation is the primary cause of an increased temperature on the plate, represented by equations (2) and (3). Literature suggests that about 90% of the total heat produced is contributed by the friction between the plate and tool [53]. As specified by equation (3), the increased temperature on the plate must be responsive to the tool's rotating speed. In the current study, the simulations were run at 800 and 1000 rpm using square and circular pin-profiled tools with similar boundary conditions. The temperature distribution over the plate during the entire process is obtained.

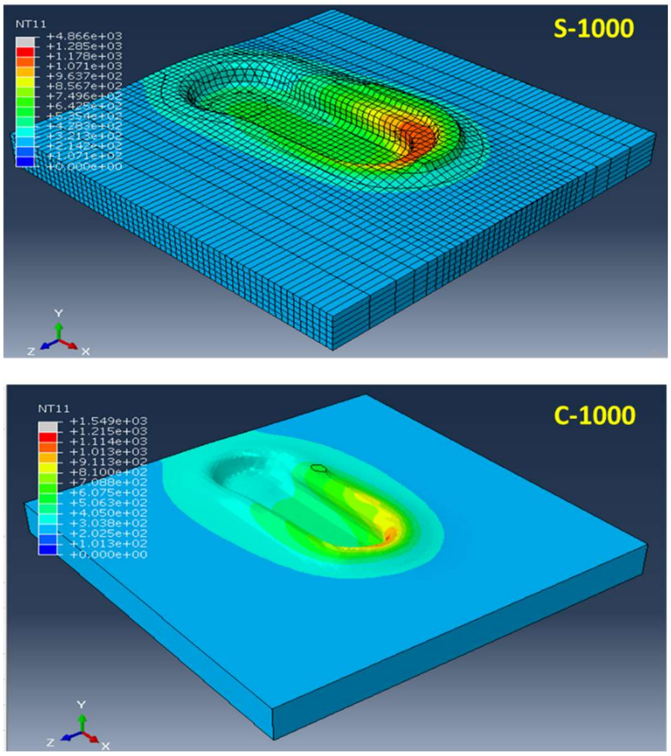

Fig.5.13: Temperature contour plots of S-1000 & C-1000

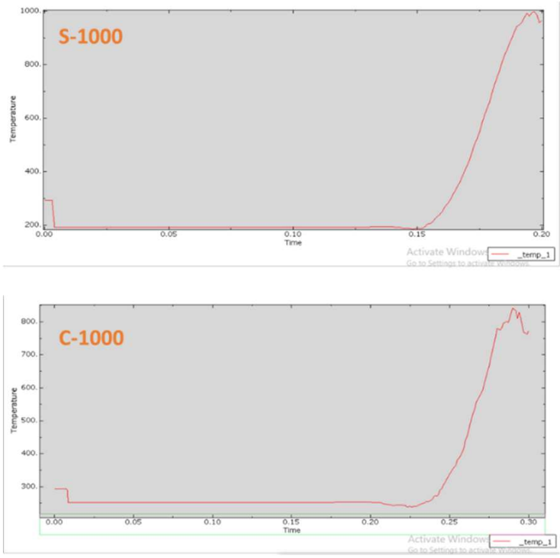

Fig.5.14: The Avg. temperature distribution in SZ at 1000 rpm

It is noticed that as the rotational speed rises, peak temperature increases and the temperature is more incase of square profile tool than circular pin profile due to pulsating action. The peak temperature was below the melting point of Al0.3CoCrFeNi HEA throughout the process. The shoulder makes contact with the plate at 0.08 sec, causing the temperature to surge rapidly. According to the literature, the shoulder supplies roughly 85-87 percent of total frictional heat[54].

At the time step of 0.2, i.e., after FSP, the average temperature is computed in the stir zone by taking 100 elements. The average temperature distribution is plotted for each processing condition.

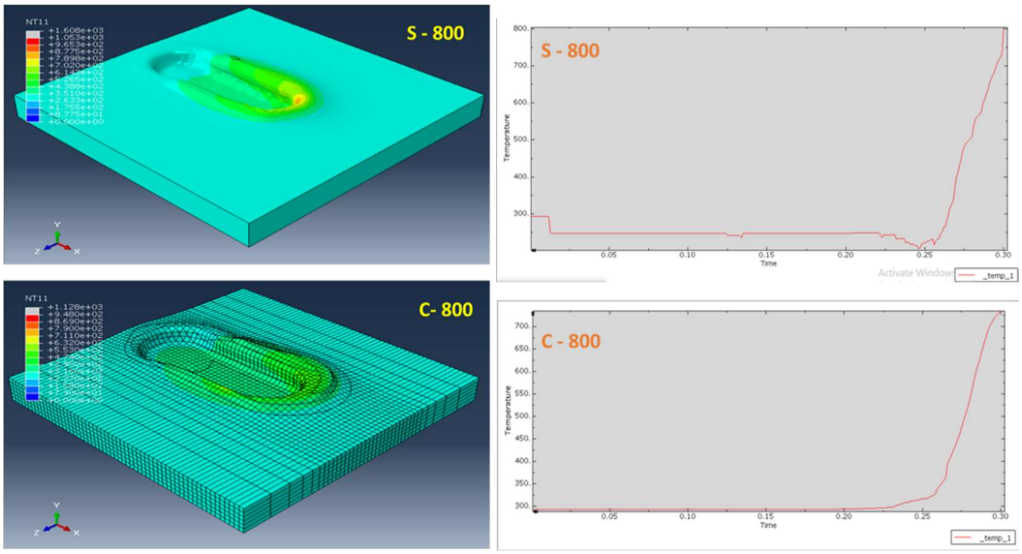

Fig.5.15: Temperature contour plots & The Avg. temperature distribution in SZ of S-800 & C-800

5.6.2 Stress Distribution:

For each processing condition, the contour profiles of Von-Mises stress are generated. As the plunging period ends and the idle period begins, stress readings start to settle. During the dwell period, stress levels are even reduced in some areas. According to Salloomi et al., the stagnation and decrease in stresses are caused by local material softening due to increased temperatures in the stir zone [53].

At the time step of 0.2, i.e., at the end of the process, the average stress distribution is calculated in the stir zone by taking 100 elements. The average stress distribution is plotted for each processing condition.

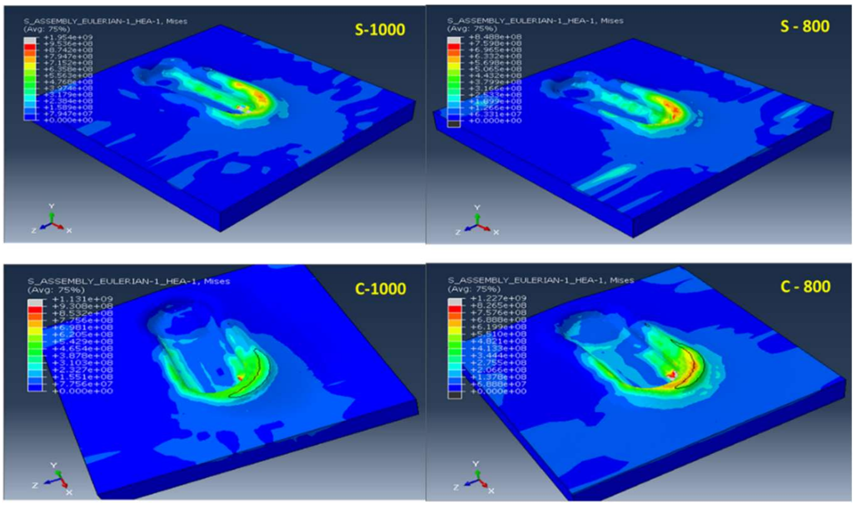

Fig. 5.16: Stress contour plots of S-1000 & C-1000

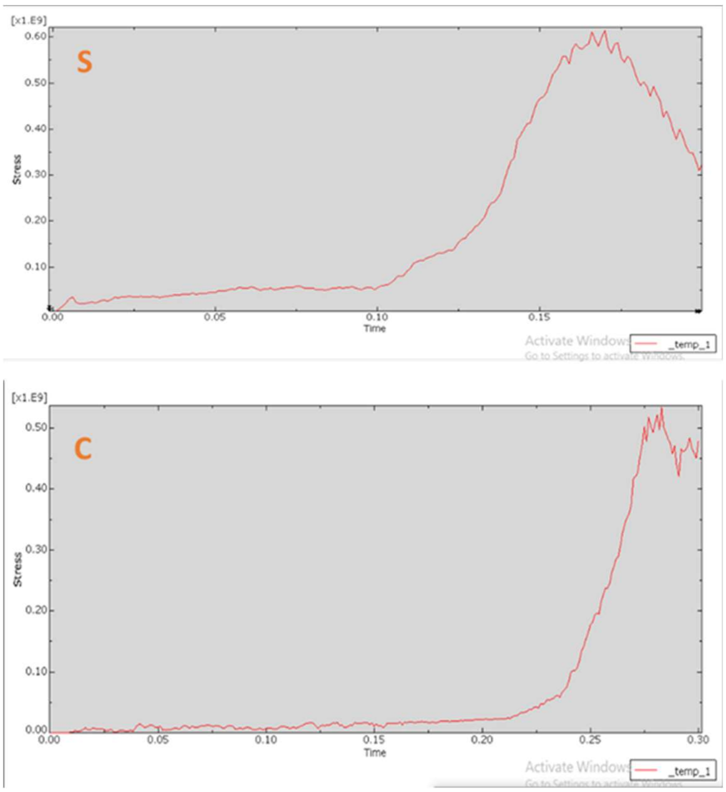

Fig.5.17: The Avg. Stress distribution in SZ

Chapter 6

Conclusions and Future Scope

6.1 Conclusions

The current research focuses on the impact of process parameters like rotational speed & pin geometry on mechanical properties and microstructural behaviour. A total of 4 experiments are conducted (S-1000, S-800, C-1000 & C-800) to investigate the effect on properties. The metallographic analysis, micro-hardness, micro-tensile tests, and numerical study are conducted to evaluate the mechanical properties. This preliminary investigation of Friction stir processing (FSP) of $Al_{0.3}CoCrFeNi$ HEA is presented in the thesis. The following conclusions could be made based on the findings and outcomes of the current research work:

- ❖ FSP is a thermo-mechanical processing technique where significant grain refinement is achieved from several millimeters to the micron level.
- ❖ The obtained results indicate that the process parameters like rotating speed & pin geometry significantly impact the resulting microstructure and mechanical characteristics.
- ❖ In the current study, the square profiled pin tool achieved a defect-free FSPed area with significant properties enhancement at 800 rpm.
- ❖ The WC fabricated tool of square pin profile and circular pin profile is found to be an appropriate tool material and tool shape for efficient FSP of $Al_{0.3}CoCrFeNi$ HEA.

- Both experimental and numerical analysis revealed that as the tool's rotating speed rises, the maximum temperature rises during FSP regardless of tool pin geometry.
- From the temperature profile, it is clear that for the same combination of process parameters like rotating & traversal speeds and plunge rate, the peak temperature is more in the case of a square profile tool than in a circular profile tool due to pulsating action.
- The metallographic analysis revealed that more refined grains are obtained using square pin geometry in the stirring zone than circular pin geometry.
- As the rotating speed increases, the hardness value decreases due to the grain growth. The highest hardness value is obtained by using the square pin profile tool.
- Out of the four processing conditions (S-1000, S-800, C-1000 & C-800), the S-800 produced a processed area with the highest hardness, UTS, and % of elongation of values 399 Hv, 665.25 MPa, and 28.7 %.
- The Yield strength and UTS of the processed material improved vastly, while ductility was slightly enhanced.
- Following FSP, the hardness of the material is substantially improved by a factor of 2.6 using a square profile pin. The asymmetry in the hardness profile is observed due to the different microstructural features across the stirring zone.

6.2 Future Scope:

The current study demonstrates the potential of this technique and $Al_{0.3}CoCrFeNi$ HEA. The numerous aspects of the FSP process can be studied further in establishing an empirical relationship between process parameters and mechanical properties.

- The tool traverse speed and plunge rate are also essential factors in resulting mechanical properties and microstructural behaviour, which are assumed to be constant in the current study.
- FSP is carried out in the current study at two rotational speeds, namely 800 and 1000 rpm. More experiments need to be conducted to develop an empirical relation between process parameters like rotational speed and pin geometry on mechanical behaviour.
- The obtained numerical results in the current study are preliminary and are further investigated to get accurate results.
- The FSP is heavily influenced by the tool design and material. Hence, the tool design modifications could be another area of research.
- The obtained numerical results like temperature profile and stress distribution during FSP need to be validated with the experimental results.

References

[1] The Traditional Medicine and Modern Medicine from Natural Products, Haidan Yuan 1,2, Qianqian Ma 1, Li Ye 1 and Guangchun Piao 1,2,*

[2] Jien-Wei Yeh, "Recent Progress in High-entropy Alloys", Annales De Chimie – Science des Materiaux, 31(2006), pp. 633-648.

[3] R. Kelsall, I. Hamley, M. Geoghegan, Nanoscale Science and Technology, John Wiley & Sons, Ltd., Weat Sussex, England, 2005.

[4] J. W. Yeh, S. K. Chen, S. J. Lin, J. Y. Gan, T. S. Chin, T. T. Shun, C. H. Tsau, and S. Y. Chang, Nanostructured High-entropy Alloys with Multi-Principal Elements—Novel Alloy Design Concepts and Outcomes, Adv. Eng. Mat., 6(5) (2004) 299-303.

[5] C.Y. Hsu, J.W. Yeh, S.K. Chen, and T.T. Shun, Wear Resistance and High-Temperature Compression Strength of FCC CuCoNiCrAl0.5Fe Alloy with Boron Addition, Metall. Mat. Trans. A, 35A (2004) 1465-1469.

[6] C.J. Tong, S.K. Chen, J.W. Yeh, T.T. Shun, C.H. Tsau, S.J. Lin, and S.Y. Chang, Microstructure Characterization of AlxCoCrCuFeNi High-Entropy Alloy System with Multi-principal Elements, Metall. Mat. Trans. A, 36A (2005) 881-893.

[7] C.J. Tong, M.R. Chen, S.K. Chen, J.W. Yeh, T.T. Shun, S.J. Lin, and S.Y. Chang, Mechanical Performance of Nanostructured AlxCoCrCuFeNi High-Entropy Alloy System with Multi-principal Elements, Metall. Mat. Trans. A, 36A (2005) 1263-1271.

[8] J.M. Wu, S.J. Lin, J.W. Yeh, S.K. Chen, and Y.S. Huang, H.C. Chen, Adhesive Wear Behavior of AlxCoCrCuFeNi High-Entropy Alloys as a Function of Aluminum Content, Wear, 261 (2006) 513-519.

[9] High-entropy alloys: a critical assessment of their founding principles and future prospects, E. J. Pickering & N. G. Jones.

[10] A critical review of high entropy alloys and related concepts D.B. Miracle a, *, O.N. Senkov a, b.

[11] High-entropy alloy: challenges and prospects Y.F. Ye, Q. Wang, J. Lu, C.T. Liu, and Y. Yang.

[12] High-entropy alloys Easo P. George 1,2*, Dierk Raabe3 and Robert O. Ritchie 4,5

[13] High-entropy alloys: emerging materials for advanced functional applications, Xin Wang, Wei Guo, and Yongzhu Fu

[14] Severe plastic deformation (SPD) processes for metals, A. Azushima (1)a, *, R. Kopp (1)b, A. Korhonen (1)c, D.Y. Yang (1)d, F. Micari (1)e, G.D. Lahoti (1)f, P. Groche (2)g, J. Yanagimoto (2)h, N. Tsuji i, A. Rosochowski j, A. Yanagida a.

[15] Kapoor, Rajeev. (2017). Severe Plastic Deformation of Materials. 10.1016/B978-0-12-801300-7.00020-6.

[16] Comparison of different methods of Severe Plastic Deformation for grain refinement Krishna Mohan Agarwal1, *, R K Tyagi1, V K Chaubey2, Anurag Dixit 3.

[17] An overview on severe plastic deformation: research status, techniques classification, microstructure evolution and applications E. Bagherpour1, N. Pardis1, M. Reihanian∗2, R. Ebrahimi1.

[18] Zrnik, Jozef & Dobatkin, Sergey & I, Mamuzić. (2008). Processing of metals by severe plastic deformation (SPD) - Structure and mechanical properties respond. Metalurgija. 47.

[19] O. S. Salih, H. Ou, W. Sun, and D. G. Mccartney, 2015. “A review of friction stir welding of aluminium matrix composites,” JMADE, vol. 86, pp. 61–71.

[20] Research Status and Prospect of Friction Stir Processing Technology Kan Li, Xuemei Liu * and Yi Zhao

[21] Heidarzadeh, A., Jabbari, M., Esmaily, M., 2014. “Prediction of grain size and mechanical properties in friction stir welded pure copper 61 joints using a thermal model”, Int. J. Adv. Manuf. Technol., Vol. 15, pp. 1–11.

[22] Balasubramanian, V., 2008. “Relationship between base metal properties and friction stir welding process parameters”, Mat. Sci. Eng. A, Vol. 480, pp.397–403.

[23] Soleymani, S., Abdollah-zadeh, A., Alidokht, S.A., 2012. “Microstructural and tribological properties of Al5083 based surface

hybrid composite produced by friction stir processing”, Wear, Vol. 278, pp. 41–47.

[24] Dolatkhah, A., Golbabaei, P., Givi, M.K.B., Molaiekiya, F., 2012. “Investigating effects of process parameters on microstructural and mechanical properties of Al5052/SiC metal matrix composite fabricated via friction stir processing”, Mater. Design, Vol. 37, pp. 458–464.

[25] Moghaddas, M.A., Kashani-Bozorg, S.F., 2013. “Effects of thermal conditions on microstructure in nanocomposite of Al/Si3N4 produced by friction stir processing”, Mater. Sci. Eng. A Vol. 559, pp. 187–193.

[26] Arbegast, W.J., Hartley, P.J., 1998. “Friction stir weld technology development at Lockheed martin Michoud space system- An overview,” Pine Mountain, GA, USA, Vol.8, pp. 541–546.

[27] Mishra, R.S., Ma, Z.Y., Charit, I., 2003. “Friction stir processing: a novel technique for fabrication of surface composite”, Mater. Sci. Eng. A, Vol. 341, pp. 307–310

[28] Palanivel, R., Koshy Mathews, P., Murugan, N., Dinaharan, I., 2012. “Effect of tool rotational speed and pin profile on microstructure and tensile strength of dissimilar friction stir welded AA5083-H111 and AA6351-T6 aluminum alloys”, Mater. Design, Vol. 40, pp. 7–16.

[29] N. Pathak, K. Bandyopadhyay, M. Sarangi, Sushanta Kumar Panda (2013). Microstructure and Mechanical Performance of Friction Stir Spot-Welded Aluminum-5754 Sheets. , 22(1), 131–144.

[30] Yutaka S. Sato; Mitsunori Urata; Hiroyuki Kokawa (2002). Parameters controlling microstructure and hardness during friction-stir welding of precipitation-hardenable aluminum alloy 6063.

[31] Effect of friction stir processing on microstructure and mechanical properties of aluminium Devinder Yadav, Ranjit Bauri ∗

[32] B.M. Darras; M.K. Khraisheh; F.K. Abu-Farha; M.A. Omar (2007). Friction stir processing of commercial AZ31 magnesium alloy. , 191(1-3), 77–81.

[33] Feng, Xiuli; Liu, Huijie; Lippold, John C. (2013). Microstructure characterization of the stir zone of submerged friction stir processed aluminum alloy 2219.

[34] Effect of process parameters on microstructure and mechanical properties of friction stir welded CoCrFeNi high entropy alloy Xiaomeng Qin a, Yi Xu a, Yufeng Sun b,c, Hidetoshi Fujii b, Zhiguang Zhu d, Chan Hung Shek a,*.

[35] An investigation of the microstructural effects on the mechanical and electrochemical properties of a friction stir processed equiatomic CrMnFeCoNi high entropy alloy Sam Yaw Anaman; Solomon Ansah; Hoon-Hwe Cho; Min-Gu Jo; Jin-Yoo Suh; Minjung Kang; Jong-Sook Lee; Sung-Tae Hong; Heung Nam Han; (2021).

[36] Achieving a High-Strength CoCrFeNiCu High-Entropy Alloy with an Ultrafine-Grained Structure via Friction Stir Processing Ning Li, Cun-Lei Jia, Zhi-Wei Wang, Li-Hui Wu, Ding-Rui Ni, Zheng-Kun Li, Hua-Meng Fu, Peng Xue, Bo-Lv Xiao, Zong-Yi Ma, Yi Shao & Yun-Long Chang.

[37] Effects of nitrogen alloying and friction stir processing on the microstructures and mechanical properties, CoCrFeMnNi high-entropy alloys, Feng Xiong, Rui-dong Fu, Yi-jun Li, De-li Sang.

[38] Effect of Microstructure on the Deformation Mechanism of Friction Stir-Processed Al0.1CoCrFeNi High Entropy Alloy M. Komarasamya, N. Kumara, Z. Tang, R.S. Mishra∗, and P.K. Liaw.

[39] S. Z. Aljoaba; I. S. Jawahir; O. W. Dillon; M. H. Ali; M. K. Khraisheh (2009). Modeling of friction stir processing using 3D CFD analysis. 2(1 Supplement), 315–318.

[40] Numerical Simulation of the Friction Stir Welding Process Using Coupled Eulerian Lagrangian Method M Iordache 1, C Badulescu 2, D Iacomi1, E Nitu 1, C Ciuca 3.

[41] Numerically modelled study of the plunge stage in friction stir spot welding using multi-tiered mesh partitions Arindam Baruah, Jayaprakash Murugesan, and Hemant Borkar.

[42] Numerical studies on controlling of process parameters in friction stir welding Z. Zhang∗, H.W. Zhang.

[43] Nonlinear Finite Element Simulation of Friction Stir Processing of Marine Grade 5083 Aluminum Alloy Emad Eldin M. KISHTA, Farid H. ABED, Basil M. DARRAS.

[44] Pierpaolo Carlone, Gaetano S. Palazzo (2013). Influence of Process Parameters on Microstructure and Mechanical Properties in AA2024-T3 Friction Stir Welding.

[45] S. Z. Aljoaba; I. S. Jawahir; O. W. Dillon; M. H. Ali; M. K. Khraisheh (2009). Modeling of friction stir processing using 3D CFD analysis. 2(1 Supplement), 315–318.

[46] Seliger, Günther; Khraisheh, Marwan M.K.; Jawahir, I.S. (2011). Advances in Sustainable Manufacturing || Modelling of Friction Stir Processing with in Process Cooling Using Computational Fluid Dynamics Analysis.

[47] Zhenzhen Yu; Wei Zhang; Hahn Choo; Zhili Feng (2012). Transient Heat and Material Flow Modeling of Friction Stir Processing of Magnesium Alloy using Threaded Tool. , 43(2), 724–737.

[48] Influences of tool pin profile and axial force on the formation of friction stir processing zone in AA6061 aluminium alloy, K. Elangovan & V. Balasubramanian & M. Valliappan.

[49] Influences of pin profile and rotational speed of the tool on the formation of friction stir processing zone in AA2219 aluminium alloy, K. Elangovan, V. Balasubramanian ∗.

[50] Influence of Pin Profile on the Tool Plunge Stage in Friction Stir Processing of Al–Zn–Mg–Cu Alloy, Vivek V. Patel1 • Vishvesh J. Badheka1 • Abhishek Kumar1.

[51] Effect of tool pin design on the microstructural evolutions and tribological characteristics of friction stir processed structural steel, Ameneh Amirafshar a,b , Ameneh Amirafshar a,b .

[52] Callister WD. 2003. An introduction. The United States of America: John Wiley & Son . pp. 153–64.

[53] Salloomi KN, Hussein FI and Al-Sumaidae SNM, Temperature and Stress Evaluation during Three Different Phases of Friction Stir Welding of AA 7075-T651 Alloy, Modelling, and Simulation in Engineering, 2020, Article ID 3197813.

[54] Schmidt H, Hattel JH, and Wert J, An analytical model for the heat generation in friction stir welding, 2003, Modelling and Simulation in Materials Science and Engineering, 12, 143.